

Discovery and Clinical Evaluation of 1-*N*-[2-(Amidinoaminoxy)ethyl]amino}carbonylmethyl-6-methyl-3-[2,2-difluoro-2-phenylethylamino]pyrazinone (RWJ-671818), a Thrombin Inhibitor with an Oxyguanidine P1 Motif

Tianbao Lu, Thomas Markotan, Shelley K. Ballentine, Edward C. Giardino, John Spurlino, Kathryn Brown, Bruce E. Maryanoff, Bruce E. Tomczuk, Bruce P. Damiano, Umesh Shukla, David End, Patricia Andrade-Gordon, Roger F. Bone, and Mark R. Player*

Johnson & Johnson Pharmaceutical Research and Development, Welsh and McKean Roads, Spring House, Pennsylvania 19477-0776

Received December 4, 2009

We have identified RWJ-671818 (**8**) as a novel, low molecular weight, orally active inhibitor of human α -thrombin ($K_i = 1.3$ nM) that is potentially useful for the acute and chronic treatment of venous and arterial thrombosis. In a rat deep venous thrombosis model used to assess antithrombotic efficacy, oral administration of **8** at 30 and 50 mg/kg reduced thrombus weight by 87 and 94%, respectively. In an anesthetized rat antithrombotic model, where electrical stimulation of the carotid artery created a thrombus, **8** prolonged occlusion time 2- and 3-fold at 0.1 and 1.0 mg/kg, iv, respectively, and more than doubled activated clotting time and activated partial thromboplastin time at the higher dose. This compound had excellent oral bioavailability of 100% in dogs with an estimated half-life of approximately 3 h. On the basis of its noteworthy preclinical data, **8** was advanced into human clinical trials and successfully progressed through phase 1 studies.

Introduction

Thromboembolic diseases remain a leading cause of morbidity and mortality in the developed world. Venous thromboembolism (VTE)¹ affects more than 2 million people in the United States each year, progressing to pulmonary embolism in approximately 600 000 of these patients and becoming fatal in 200 000.¹ VTE is the third leading cause of cardiovascular-related death, after myocardial infarction and stroke.² Nonvalvular atrial fibrillation is among the most common dysrhythmia seen in clinical practice and is responsible for up to 100 000 ischemic strokes annually in the United States and more than a million worldwide.³

The conditions amenable to treatment with anticoagulants are broad, reflecting the importance of thrombosis in pathophysiology. They include the following: primary prevention of acute myocardial infarction, stroke, and cerebral ischemia; treatment of unstable angina; prevention of occlusion following percutaneous transluminal coronary angioplasty and coronary artery bypass grafting; prevention of reocclusion after acute coronary intervention using intravascular stents;

prevention of systemic thrombosis after heart valve replacement or atrial fibrillation; and treatment and prevention of all forms of VTE [deep venous thrombosis (DVT), pulmonary embolism, and disseminated intravascular coagulation], secondary myocardial infarction, and restenosis.

Anticoagulants have great promise for the prophylaxis of arterial and venous thrombotic disorders. Injectable agents have been in use since unfractionated heparin became commercially available in the 1940s. Low molecular weight heparins were developed in the early 1990s. The first direct thrombin inhibitor (DTI) was introduced in 1998, and the first synthetic indirect factor Xa (fXa) inhibitor, fondaparinux, became available in 2001. However, until very recently, oral agents have been limited to vitamin K antagonists such as warfarin. Vitamin K antagonists are highly efficacious but suffer from a slow onset of action, genetic variations of metabolism, complex food and drug interactions, and the costly requirement of monitoring for dose adjustments. Thus, there is a significant unmet need for new oral anticoagulants with rapid onset of action and predictable pharmacokinetics and pharmacodynamics.

The central role of the serine protease thrombin in thrombosis and hemostasis⁴ makes it an attractive target for antithrombotic therapy. As a key enzyme in the blood coagulation pathway, thrombin acts on substrates such as fibrinogen, factor V, factor VIII, factor XI, and factor XIII to induce or accelerate the formation of thrombi.⁴ Thrombin very efficiently initiates fibrin formation and activates factor XIII, a transglutaminase that catalyzes the formation of cross-links between fibrin monomers. In addition, thrombin effectively promotes platelet activation via enzymatic cleavage of the amino terminus of protease-activated receptors (PARs) on the platelet surface (PAR-1, PAR-3, and PAR-4), unveiling a

*To whom correspondence should be addressed. Tel: 215-628-7860. Fax: 215-540-4616. E-mail: mplayer@its.jnj.com.

^aAbbreviations: ACT, activated clotting time; aPTT, activated partial thromboplastin time; argatroban, (2*R*,4*R*)-1-[(2*S*)-5-(diaminomethylideneamino)-2-[[[(3*R*)-3-methyl-1,2,3,4-tetrahydroquinolin-8-yl]sulfonylamino]pentanoyl]-4-methyl-piperidine-2-carboxylic acid; BOP, benzotriazole-1-yl-oxy-tris-(dimethylamino)-phosphonium hexafluorophosphate; CYP, cytochrome P450; DTI, direct thrombin inhibitor; DVT, deep venous thrombosis; ECAT, electrical current-induced arterial thrombosis; fXa, factor Xa; hERG, human ether-a-go-go related gene; HLM, human liver microsome; PAR, protease-activated receptor; PT, prothrombin time; RGD, arginine-glycine-aspartic acid; RLM, rat liver microsome; VTE, venous thromboembolism.

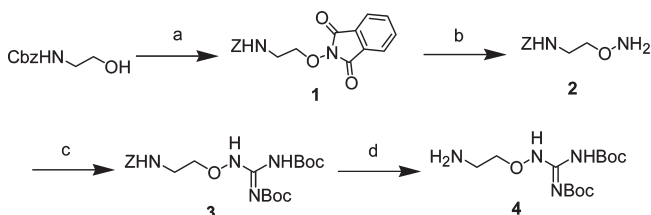
tethered receptor ligand mechanism, which in turn activates the receptor to elicit platelet activation. For example, mice deficient in PAR-4 demonstrate reduced thrombus formation at sites of arterial injury.⁵ In contrast, through its interaction with thrombomodulin, thrombin activates protein C, initiating negative feedback of the coagulation cascade. Activated protein C inactivates factors Va and VIIIa and regulates fibrinolysis via activation of a fibrinolysis inhibitor.⁶ Anti-thrombin is the physiological inhibitor of thrombin; however, thrombin bound to a fibrin clot is inaccessible to the actions of antithrombin. Thrombin, via activation of PARs, is also a modulator of endothelial and smooth muscle cell proliferation and migration. It induces inflammatory responses, acting as a chemotactic to peripheral blood monocytes and as a stimulator of neutrophil adhesion.⁷ Thus, a potent inhibitor of thrombin has potential as an effective antithrombotic drug in both venous and arterial environments. Herein, we describe a series of potent pyrazinone thrombin inhibitors, which culminated in the discovery and clinical evaluation of **8**.

Results and Discussion

Synthetic Chemistry. Preparation of the P1 intermediate **4** (Scheme 1) started with the reaction of (2-hydroxy-ethyl)-carbamic acid benzyl ester with *N*-hydroxyphthalimide to afford **1**, which was deprotected with methylamine to give oxyamine **2**. Guanylation of **2** provided the bis-BOC intermediate **3**, which was deprotected to afford key intermediate oxyguanidine **4** in 49% overall yield beginning with the alcohol.

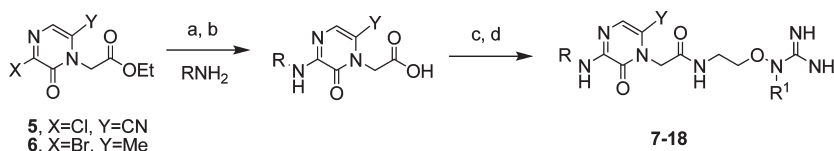
Reaction of 3-halo-6-substituted pyrazinone intermediates **5**^{16b} and **6**⁸ (Scheme 2) with the appropriate alkylamine

Scheme 1^a



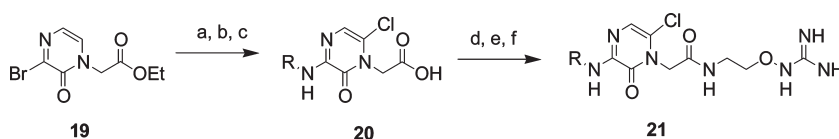
^a Reagents and conditions: (a) *N*-Hydroxyphthalimide, PPh₃, DEAD, room temperature, 10 h. (b) MeNH₂, EtOH/THF, room temperature, 1 h. (c) [*N,N'*-Di(*tert*-butoxycarbonyl)]amidinopyrazole, room temperature, 10 h. (d) 10% Pd/C, H₂(g), EtOH/THF, room temperature, 30 min.

Scheme 2^a



^a Reagents and conditions: (a) PhMe, 60 °C, 3 h. (b) (i) Dioxane/1 N NaOH(aq), room temperature, 1.5 h; (ii) 10% HCl(aq). (c) Castro's reagent, TEA, DMF, room temperature, 18 h. (d) DCM, TFA, room temperature, 8 h.

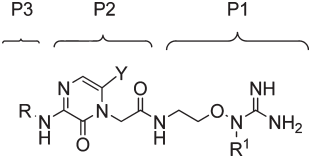
Scheme 3^a



^a Reagents and conditions: (a) PhMe, reflux, 12 h and then room temperature, 5 days. (b) NCS, DCE, reflux, 2.5 h. (c) (i) dioxane/1 N NaOH(aq), room temperature, 18 h; (ii) 10% HCl(aq). (d) Castro's reagent, TEA, DMF, room temperature, 3 days. (e) DCM, TFA, room temperature, 24 h.

in refluxing toluene followed by saponification provided the 3-alkylamino-6-substituted pyrazinone acetic acids. The coupling of the acid and oxyguanidine intermediate **4** was accomplished with benzotriazole-1-yl-oxy-tris-(dimethylamino)-phosphonium hexafluorophosphate (BOP). The crude coupling product was purified by normal phase chromatography and then deprotected by treatment with trifluoroacetic acid. Subsequent purification of the product by normal phase chromatography followed by recrystallization of the HCl salt from ethanol provided **7–18**. To obtain the 3-alkylamino-6-chloropyrazinone acetic acids, coupling of the amine took place with 3-bromopyrazinone acetic acid ester **19**⁹ (Scheme 3) in refluxing toluene followed by chlorination using *N*-chlorosuccinimide, and subsequent saponification afforded **20**. Installation of the P1 oxyguanidine then took place in an analogous manner as described for **7–18**. Methylation of the oxyguanidine on the proximal nitrogen was accomplished using iodomethane to yield **22**.

Ligand Design. Many early approaches to thrombin inhibitors relied upon the active site recognition motif D-Phe-Pro-Arg, which mimics a portion of the natural substrate.¹⁰ Each inhibitor may be thought of as being composed of three components: a basic P1 substituent, a central group that acts as a scaffold and/or S2 binding fragment, and an aryl substituent, P3. Modeling studies¹¹ involving the docking of a similar inhibitor Ac-Ala-Pro-Val-TFMK (trifluoromethylketone) into the active site of human neutrophil elastase suggested that it might be possible to alter the alanine α -carbon hybridization from sp³ to sp² and construct a hydrocarbon bridge from it to the adjacent proline. This modification, combined with cleavage and deletion of two carbons of the proline ring, results in a substituted pyridone that retains many of the important hydrogen bond recognition elements of the tripeptides. However, many 3-amino-2-pyridones show inherent chemical instability due to the electron-rich nature of the pyridone ring.¹² Stabilization of the heterocycle has been addressed in three ways: insertion of a strongly electron-withdrawing substituent such as CF₃ at the 4-position, derivatization of the 3-amino group as a sulfonamide, or addition of a nitrogen to convert the pyridone into a pyrazinone core.¹¹ These strategies, particularly the conversion to a pyrazinone core, are applicable to thrombin inhibitors and have been used to design compounds with a balance of thrombin affinity and physical properties that permit desirable pharmacokinetics.

Table 1. Effect of P1–P3 Substitution on Thrombin (thr) and Trypsin (tryp) Inhibition (K_i) of 7–18, 21, and 22


compd	R	Y	R ¹	thr K_i ^a (nM)	tryp K_i (nM)
7	2,2-difluoro-2-phenylethyl	CN	H	2.3	105
8	2,2-difluoro-2-phenylethyl	Me	H	1.3	128
9	2-(4-fluorophenyl)ethyl	Me	H	13	1600
10	2-(3,4-difluorophenyl)ethyl	Me	H	47	850
11	2-(2,4-difluorophenyl)ethyl	Me	H	15	3400
12	2-(4-trifluoromethylphenyl)ethyl	Me	H	47	2800
13	2-(4-methoxyphenyl)ethyl	Me	H	11	3000
14	2-(3,4-dimethoxyphenyl)ethyl	Me	H	120	3100
15	2-(4-ethylphenyl)ethyl	Me	H	66	2200
16	2-(5-indanyl)ethyl	Me	H	44	2500
17	2-(1-naphthyl)ethyl	Me	H	12	500
18	2,2-diphenylethyl	Me	H	6.8	420
21	2,2-difluoro-2-phenylethyl	Cl	H	1.7	370
22	2-(4-methylphenyl)ethyl	Me	Me	37	2500

^a K_i values are averaged from multiple determinations ($n \geq 3$), and the standard deviations are <20% of the mean.

Arginine- or guanidine-based P1 groups provide molecules with high affinity by virtue of a strong salt bridge interaction with Asp189 in the S1 specificity pocket. The strong basicity of such groups, however, often causes low oral bioavailability due to poor intestinal absorption. In addition, some inhibitors with aminocyclohexane P1s display in vivo toxicity, the severity of which is a direct function of the pK_a of the aminocyclohexane.¹³ To address these problems, we have previously reported on a series of thrombin inhibitors exhibiting a novel oxyguanidine moiety, which serves as an arginine surrogate of the arginine-glycine-aspartic acid (RGD) type thrombin inhibitors.¹⁴ The oxyguanidine possesses a greatly reduced pK_a of 7.0–7.5 versus 13–14 for guanidine, and this distinguishing characteristic is reflected in favorable in vitro permeability and pharmacokinetics. The current series combines the features of the pyrazinone core with the oxyguanidine moiety.

Structure–Activity Study. We conducted a survey of a variety of lipophilic P3 substituents on the pyrazinone core. The effects of methyl, chloro, and cyano substitution on the 6-position of the pyrazinone ring were also addressed. A range of compounds (7–18, 21, and 22) were assessed for the inhibition of human α -thrombin and the key enzyme trypsin (Table 1). Insights emerged regarding the effect of P3 group substitution on thrombin binding and on selectivity with respect to trypsin. 2-(4-Fluorophenyl)ethyl compound **9** ($K_i = 13$ nM) was essentially equipotent to **11** ($K_i = 15$ nM), a 2,4-difluoro-substituted analogue; however, 3,4-difluoro-substitution, as in **10**, decreased the potency 3-fold ($K_i = 47$ nM). The substitution pattern more significantly affected the selectivity of this set of compounds against trypsin, however: **10**, **9**, and **11** were 18-, 120-, and 230-fold more potent for thrombin than for trypsin. The same preference for monosubstitution as compared to 3,4-substitution was seen in methoxy derivatives **13** and **14**, which exhibited K_i values of 11 and 120 nM, respectively. Although it has been hypothesized that electron-withdrawing substituents on P3 decrease electron density in the

Table 2. Rat and Human Microsomal Stability, Caco-2 Flux, and Recombinant CYP3A4 Inhibition of 7–18, 21, and 22

compd	$t_{1/2}$ (min)		Caco-2 P_{app} (A→B/B→A) ($\times 10^{-6}$ cm/s)	CYP3A4 inhibition (μ M)
	RLM stability	HLM stability		
7	>100	>100	0.5, 2.26	>10
8	>100	>100	1.37, 6.45	>10
9	16.7	40.1	0.55, 1.48	5.9
10	13.8	85.8	0.92, 1.84	2.1
11	14.4	57.6	0.5, 1.91	2.9
12	44.7	16.6	0.74, 3.32	3.0
13	32.9	19.1	0.28, 3.18	3.5
14	>10	34.1	0.87, 0.36	6.7
15	52.3	24.5	0.29, 10.3	3.4
16	32.6	22.8	0.67, 4.29	4.7
17	38.8	24.4	0.32, 11.81	0.96
18	8.3	25.9	0.14, 12.98	1.2
21	17.7	>100	0.5, 3.04	1.5
22	24.8	59.2	0.27, 0.6	3.5

aromatic ring and thereby enhance the σ – π edge-to-face interaction of the ring with the protein at electron-rich Trp215,¹⁵ in this series, such a change was not beneficial, as demonstrated by the 4-trifluoromethyl analogue **12** ($K_i = 47$ nM). Further comparing compounds with different inductive effects at the 4-position, the trend in K_i values was OMe (**13**) < F (**9**) < CF₃ (**12**) < ethyl (**15**) (11, 13, 47, and 66 nM, respectively). The potencies of these substitutions are likely due to their presence only at the 4-position, allowing a slight structural rearrangement of the binding pocket to accommodate the fit. Compound **14**, the 3,4-dimethoxy analogue, is even less potent ($K_i = 120$ nM) as it requires even more structural adjustment at the P3 site.

Analogues with larger hydrophobic substituents, such as 2,2-diphenylethyl (**18**, $K_i = 6.8$ nM), 2-(1-naphthyl)ethyl (**17**, $K_i = 12$ nM), and 4-methylphenyl (**22**, $K_i = 37$ nM) maintained potency, as they may project out of the P3 pocket into solvent. Compounds **18** and **17** concurrently displayed 62- and 4-fold selectivity over trypsin, respectively. 2-(5-Indanyl)ethyl (**16**, $K_i = 44$ nM) was approximately as potent as other 3,4-disubstituted phenyl analogues such as **10** and **14**. Compound **22** also featured a methyl group at the proximal nitrogen of the oxyguanidine (α to the oxygen), which did not negatively impact potency or selectivity over trypsin (68-fold) (vide infra).

The addition of a *gem*-difluoromethyl group on the benzylic position of the P3 moiety not only conferred greater thrombin affinity but also higher metabolic stability, as that position was shown to be one important site of oxidative metabolism.¹⁶ This phenomenon was exemplified by **7**, **8**, and **21**. They were among the most potent compounds studied, with K_i values of 2.3, 1.3, and 1.7 nM, respectively. In human liver microsomal (HLM) preparations, the half-lives of each of these three compounds exceeded 100 min (Table 2). Without this modification to attenuate the metabolic liability, half-lives shortened considerably, ranging from 16.6 min for **12** to 85.8 min for **10**. Within that range, most HLM $t_{1/2}$ values were between 20 and 30 min.

Substitution in the 6-position of the pyrazinone ring improved potency via interaction with the Tyr-Pro-Pro-Trp insertion loop near the S2 pocket of thrombin. In the past, substituents such as methyl appeared to be metabolically labile,¹⁷ although given the high rat liver microsome (RLM) and HLM half-lives, particularly of **8**, that does not appear to be the case throughout this series. Compound **21**,

which contains a 6-Cl substitution on the pyrazinone, was 1.7 nM against thrombin and 370 nM against trypsin. 6-Cyano and 6-methyl groups (**7** and **8**), despite decreasing trypsin selectivity ($K_i = 105$ and 128 nM, respectively), maintained high affinity for thrombin ($K_i = 2.3$ and 1.3 nM, respectively). The electron-withdrawing Cl and CN and the hydrophobic methyl were all well-tolerated within the relatively hydrophobic section of protein in the S2 insertion loop.

The crystal structure of **8** reveals the archetypical binding mode for the series of pyrazinone compounds. Initial difference electron density maps, calculated from atomic coordinates after positional and temperature factor refinement without the inhibitor, clearly revealed the positions of the inhibitor as well as additional solvent molecules that were not included in the difference Fourier calculation. The central pyrazinone scaffold makes hydrogen bonds with the backbone NH and CO of Gly216 as a peptide mimetic (Figure 1a,b; PDB ID: 3LDX). The methyl substitution projects into the pocket formed by His57, Tyr60A, and Trp60D, mostly filling this pocket, and there is space for the slightly larger substitutions of Cl or CN with minimal rearrangement required. The amide NH also contributes a hydrogen bond to the backbone of the protein (Ser214) to complete the scaffold interactions.

The oxyguanidine binds in an asymmetric mode to Asp189. Additional hydrogen bonds are made with the backbone carbonyl of Gly219 and two water molecules to fully coordinate the oxyguanidine moiety. Water 49 is fully coordinated making hydrogen bonds with oxygen and one of the terminal guanidine nitrogens as well as with the backbone carbonyl of Gly216. Water 3 is associated with the proximal nitrogen and the other terminal nitrogen of the guanidine. The use of water molecules to bridge hydrogen-bonding interactions with the hydrogen atom of the proximal nitrogen allows flexibility in this region of the molecule. An alternate symmetrical binding mode of an orcinol-based inhibitor with the hydrogen of the proximal nitrogen flipped was seen in a previously reported oxyguanidine structure (Figure 1c; PDB ID: 1T4U).¹⁸ This flexibility, along with the use of water-bridged hydrogen bonding, explains the ability to substitute a methyl group for the hydrogen atom on the proximal nitrogen (**22**) without a significant loss of affinity.

Selectivity for thrombin versus trypsin is important because of the central location of trypsin in the gut and its likely role in protease-mediated feedback control of endogenous pancreatic enzyme secretion.¹⁹ Recognizing that the S1 pockets of thrombin and trypsin are identical with the exception of residue 190, which is alanine and serine, respectively, one possible approach would take advantage of the slightly larger size of the pocket in thrombin by decreasing the number of hydrophilic groups and increasing the hydrophobic surface area until the limit of the pocket is reached.²⁰ Sanderson et al., utilizing this strategy, have disclosed affinity and trypsin selectivity data for related series of pyrazinone thrombin inhibitors.²¹ A lead compound, featuring an 2-amino-6-methyl pyridine at P1, had a K_i of 0.8 nM for thrombin and 1800 nM for trypsin. Other P1 groups have also been employed as follows: imidazopyridazines, 5-linked indoles, and azaindoles²¹ (the affinity of the three isomers correlates with the acidity of the conjugate acid), azoles,²² imidazole acetamides,²³ and aminopyridines.¹¹

In addition, Reiner et al. have reported pyrazinone thrombin inhibitors embodying three classes of monocyclic P1 arginine surrogates: (1) (hetero)aromatic amidines, amines,

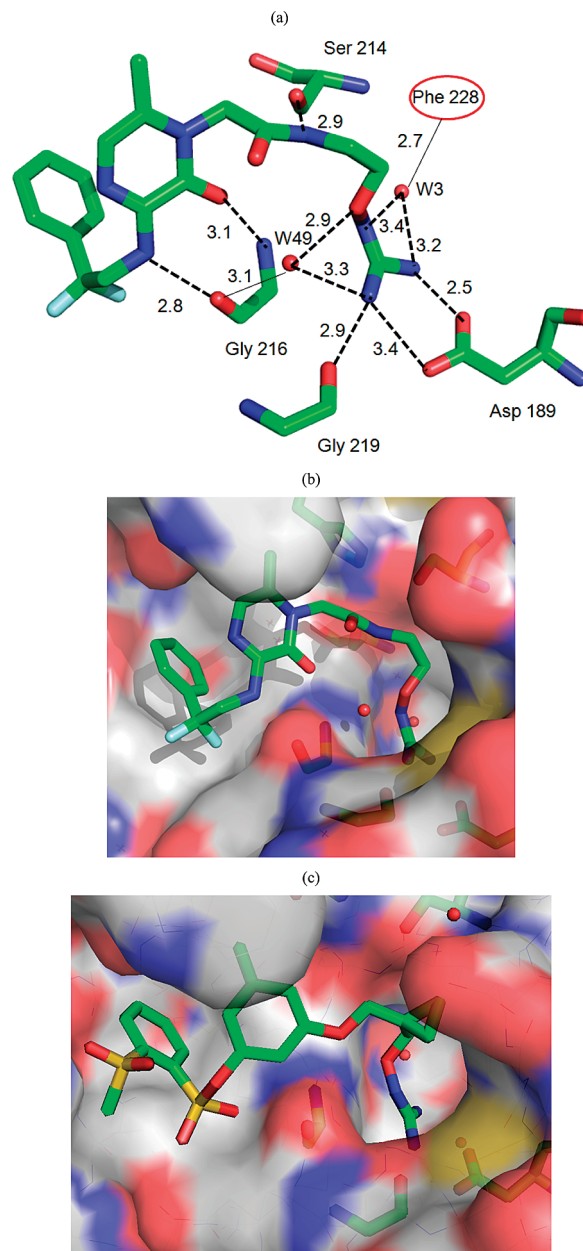


Figure 1. (a) Hydrogen-bonding interactions of **8** with thrombin (PDB ID: 3LDX). The atoms are colored by atom type. Primary interactions are shown as dotted lines, and secondary shell interactions are shown as thin solid lines. (b) Accessible surface representation of thrombin is shown with the surface colored by atom type with **8** shown as a stick representation. (c) Accessible surface representation of thrombin with the inhibitor (PDB ID: 1T4U) shown as a stick figure.

and hydroxylamines; (2) 2-aminopyrazines; and (3) 2-aminopyrimidines and 2-aminotetrahydropyrimidines.²⁴ Those containing benzylamine and thiophene were often single digit nanomolar in potency for thrombin but triple digit nanomolar for trypsin; however, those containing aminopyrimidines or aminopyrazines were considered inactive for trypsin, thus more selective.

Advanced In Vitro Evaluation. Our exploration of the space occupied by P3 led to **7**, **8**, and **21**, which were 42-, 32-, and 217-fold selective versus trypsin, respectively (Table 1). Compound **8** did have slight inhibitory potential for tissue type plasminogen activator (tPA, $K_i = 2.4 \mu\text{M}$) and fXa

Table 3. Human Plasma Protein Binding (hPPB), in Vitro Anticoagulant Potency ($2\times$ aPTT), and Rat and Dog Pharmacokinetic Parameters of **7**, **8**, and **21**

compd	hPPB (%)	$2\times$ aPTT (nM)	rat			dog		
			C_{\max} (μM) ^a	$t_{1/2}$ (h) ^b	F (%)	C_{\max} (μM) ^a	$t_{1/2}$ (h) ^b	F (%)
7	49	342	0.2	1.6	11	3.3	3.9	57
8	67	510	3.3 ^c	3.3	23	5.7	2.6	103
21	88	565	0.2	3.7	9	1.6	2.1	60

^aDose = 10 mg/kg unless otherwise noted in fasted animals. ^bpo half-life. ^cDose = 30 mg/kg.

($K_i = 3.3 \mu\text{M}$); however, the compounds were inactive ($> 26 \mu\text{M}$) against many other important enzymes, that is, factor VIIa, urokinase, chymotrypsin, cathepsin G, human leukocyte elastase, kallikrein, chymase, and plasmin. Of these, **7** had slight inhibitory potential for fXa ($K_i = 6.5 \mu\text{M}$).

Further in vitro evaluation of **7**, **8**, and **21** was undertaken to assess the metabolic stability, permeability, and recombinant cytochrome P450 (CYP) inhibition of these three lead compounds as compared to others in the series (Table 2). Test compounds were equilibrated with RLMs and HLMs at 37 °C, NADPH was added to initiate the reaction, and aliquots were withdrawn and quenched at 0, 15, 30, and 60 min. The percent of parent compound remaining in the incubation mixture was plotted as a function of time. The elimination half-lives of **7** and **8** associated with the disappearance of test article were determined to be > 100 min in both species, suggesting that **7** and **8** are not susceptible to rapid metabolism by this mechanism. The half-life for **21** was > 100 min in HLMs but dropped to 17.7 min in RLMs.

Permeability was measured by movement of compound through Caco-2 cell monolayers grown on collagen-coated, microporous, polycarbonate membranes. Compound **7** exhibited low absorption potential, having movement from apical to basolateral (A to B) of 0.5×10^{-6} cm/s and from B to A of 2.26×10^{-6} cm/s, while the absorption potential for **8** was considered high (A to B = 1.37×10^{-6} cm/s and B to A = 6.45×10^{-6} cm/s). The absorption potential for **21** was similar to that of **7** (A to B = 0.5×10^{-6} cm/s and B to A = 3.04×10^{-6} cm/s).

The HLM CYP inhibition assay was performed using cDNA-expressed human enzymes of the P450 isoforms most commonly responsible for the metabolism of drugs and associated drug–drug interactions. Of particular interest was the CYP3A4 isoform, as a few compounds in the series, including **21**, demonstrated 3A4 inhibition $\leq 3 \mu\text{M}$. The values for **7** and **8**, however, were both $> 10 \mu\text{M}$, and there was no significant inhibition of any other P450 enzyme isoform tested.

Pharmacokinetics. Table 3 summarizes the results of the plasma protein binding (PPB) and rat and dog pharmacokinetic studies for **7**, **8**, and **21**. PPB was low (49, 67, and 88%, respectively). Compound **7**, when administered to dogs at 10 mg/kg po, displayed a C_{\max} of $3.3 \mu\text{M}$, a half-life of 3.9 h, and an oral bioavailability of 57%. At the same dose level and route of administration of **8**, the C_{\max} was $5.7 \mu\text{M}$, the half-life was 2.6 h, and the oral bioavailability was 100%. In contrast, the values for **21** were $1.6 \mu\text{M}$, 2.1 h, and 60%, respectively.

Anticoagulant and Antithrombotic Studies. On the basis of the results of the aforementioned in vitro and in vivo studies, **7** and **8** were chosen for continued assessment. Activated partial thromboplastin time (aPTT) is a global clotting test sensitive to plasma concentration variations in several clotting factors, particularly factors I, V, VII, IX, and XII of the

intrinsic and common pathways, and is measured as follows: Blood samples are buffered by sodium citrate at a final concentration of 0.105–0.109 M and treated with phospholipids, surface activators, and calcium to shorten clotting time and initiate the coagulation reactions. A coagulometer is then used to measure the optical density of the mixture and record the time required to reach the threshold density at which a clot is said to have formed. Therapies prolonging aPTT from 1.5 to 2.5 (generally 2-fold) times the midpoint of the control range are associated with a reduction in the risk of recurrent thrombosis. Measurements of aPTT can be sensitive to the exact nature of the reagents used as well as sample storage/preparation protocols. Nevertheless, both prolonged and shortened aPTT values can have significant clinical implications with respect to bleeding and hypercoagulation, respectively. In the present study, fresh whole blood from humans, dogs, and rats was centrifuged to obtain plasma, and **8** was added to the plasma in concentrations from 0.001 to 100 μM . After a short stabilization period, the samples were placed in an ACL 100 micro sampler coagulation analyzer to determine clotting times in seconds. In human-, rat-, and dog-spiked plasma, **8** doubled aPTT coagulation time at concentrations of 0.51 ± 0.08 , 0.85 ± 0.12 , and $2.03 \pm 0.48 \mu\text{M}$, respectively. Compound **7** doubled aPTT coagulation time at a concentration of $0.34 \pm 0.02 \mu\text{M}$ in human plasma.

To further define the antithrombotic efficacy of **7** and **8**, an electrical current-induced arterial thrombosis (ECAT) model in rats was used to evaluate the ability of the compounds to prolong time to occlusion.²⁵ Because arterial thrombosis in humans usually occurs in areas of medium to high blood flow and high shear stress with a triggering factor of vascular injury such as atherosclerotic plaque rupture, the ECAT model may have strong pathophysiological relevance to human disease. Wong et al.^{25c} utilized scanning electron microscopy to confirm vessel wall injury at the site of electrical stimulation in this model: The de-endothelialized layer of the vessel showed both platelet and fibrin deposition, likely due to activation of the coagulation cascade by exposed tissue factor. Intravenous administration of **7** at doses of 0.03, 0.1, 0.3, and 1.0 mg/kg resulted in a prolongation of time to occlusion from a control of 11 ± 1 to 15.3 ± 3.2 , 19.3 ± 3.8 , 24.9 ± 2.6 , and 30 ± 0 min, respectively, while **8** (iv) resulted in a prolongation of time to occlusion to 18.4 ± 7.1 , 20.7 ± 3.7 , 14.7 ± 5.0 , and 30 ± 0 min, respectively (Figure 2). aPTT was also prolonged in a dose-related manner (Figure 3). For **8**, the increases in aPTT from a control of 21 ± 2 s were 23 ± 1 , 31 ± 4 , 35 ± 8 , and 66 ± 42 s, respectively. A doubling of aPTT occurred at a dose of between 0.3 to 1.0 mg/kg, which was associated with plasma concentrations of **8** between 0.12 and $0.31 \mu\text{M}$. For **7**, the increases in aPTT were 28 ± 2 , 30 ± 2 , 37 ± 9 , and 47 ± 4 s, respectively. A doubling of aPTT also occurred at a dose of between 0.3 and 1.0 mg/kg, which was associated with

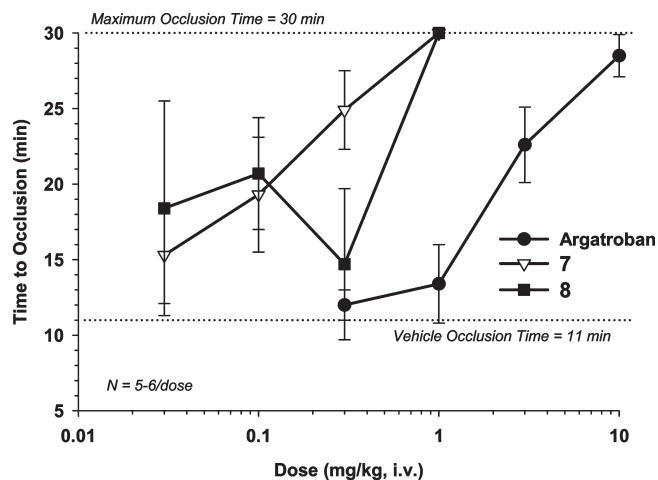


Figure 2. Time to carotid artery occlusion as a function of dose for 7 and 8 in the rat ECAT model.

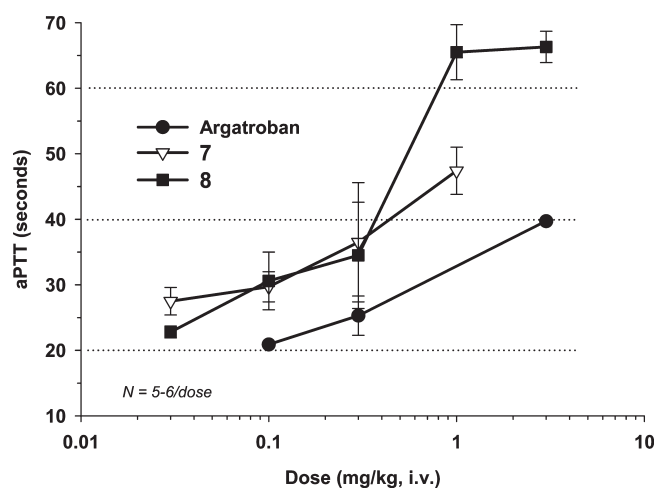


Figure 3. aPTT as a function of dose for 7 and 8 in the rat ECAT model.

plasma concentrations of 7 between 0.085 and 0.38 μM . In this model, 7 and 8 were 10-fold more potent than the reference DTI (2*R*,4*R*)-1-[(2*S*)-5(diaminomethylidene-amino)-2-[[3(*R*)-3-methyl-1,2,3,4-tetrahydroquinolin-8-yl]-sulfonylamino]pentanoyl]-4-methyl-piperidine-2-carboxylic acid (argatroban) and equipotent to one another by dose.

An arteriovenous shunt procedure was employed as a suitable model to test the antithrombotic efficacy of the two lead thrombin inhibitors against a thrombus of mixed platelet/fibrin/red blood cell composition. In this model, a thrombus forms on a section of silk thread placed in an extracorporeal shunt between the femoral artery and the vein.²⁶ Imaging studies²⁷ using a ⁹⁹Tc-labeled platelet glycoprotein IIb/IIIa receptor antagonist have shown that the deposition on the thrombogenic surface mimics a high-shear, platelet-rich thrombus indicative of arterial conditions, and the platelet-poor tail mimics that of a venous thrombus stemming from a platelet-poor, low-shear environment. Studies consisting of seven shunt periods in dogs starting at 2 h postdrug and repeating every 30 min were performed. The thrombus weight was measured after each shunt period, and bleeding times and coagulation times were measured at 2, 3, 4, and 5 h and compared to control values.

Thrombus formation (thrombus weight) by 7 was inhibited 38 ± 9 to $45 \pm 12\%$, while for 8 inhibition ranged from

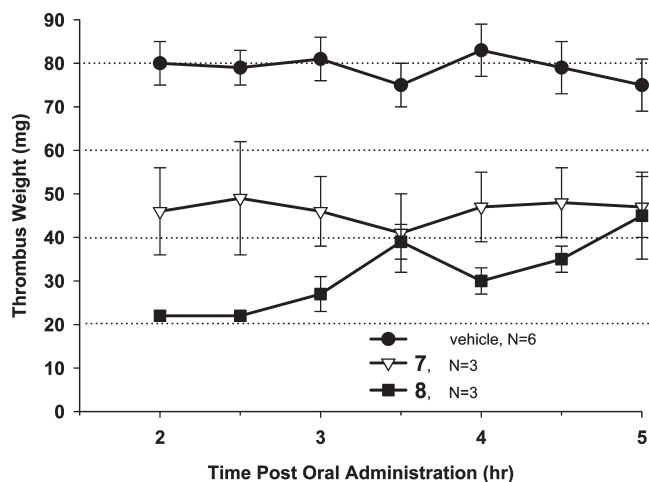


Figure 4. Antithrombotic effect of 7 and 8 after an oral dose of 3 mg/kg in the canine arteriovenous shunt model.

40 ± 13 to $73 \pm 2\%$ (Figure 4) during the 3 h testing period starting at 2 h postoral dosing. There were no significant changes in bleeding times as compared to vehicle experiments. Compound 8 administered orally at 3 mg/kg had no overt side effects in three out of three dogs during the 1 h period before they were anesthetized. aPTT was increased 1.6-fold for 8 at 1 h postoral dose as compared to 1.4-fold for 7. Plasma concentrations at the 1 h time point were $0.87 \pm 0.3 \mu\text{M}$ for 8 as compared to $0.48 \pm 0.16 \mu\text{M}$ for 7.

To further define the intravenous and oral antithrombotic efficacy of 8, a rat deep vein thrombosis model was used to evaluate the compound's ability to inhibit venous thrombus formation (Table 4).²⁸ All experimental animal models of venous thrombosis include a trigger of the thrombogenic state, which is most often composed of two components of Virchow's triad: hypercoagulability, reduced blood flow, and vessel wall injury. Hypercoagulability is induced by treatment with an agent such as tissue factor or thromboplastin. Blood flow reduction can be achieved by complete stasis, in which case the concentration of blood components and antithrombotic agent is constant within the occluded segment. Reduced blood flow may also result from a partial stasis, which allows flow of test compound and blood components around the formed thrombus. Vessel wall injury plays a major role in the partial stasis paradigm or can be generated separately by means of ferric chloride or saline. Intravenous administration of 8 resulted in a 66 and 98% inhibition in thrombus weight at the 0.3 and 1 mg/kg dose, respectively (Table 4) as well as dose-related changes in coagulation times. Oral administration of 30 and 50 mg/kg resulted in 87 and 94% inhibition of thrombus weight as well as dose-related changes in coagulation.

Cardiovascular Safety. As part of an assessment of cardiovascular safety, 8 was evaluated in vitro for its effects on the human ether-a-go-go related gene (hERG) potassium channel. In the direct hERG channel binding assay, 8 demonstrated 50% inhibition of ³H-astemizole binding at 10 μM . However, in an assay measuring percent inhibition of the Ikr-like current in hERG-transfected human embryonic kidney cells, 8 had only a minimal effect, showing a mean value of $9 \pm 2\%$, which suggests that it has limited functional activity and should not cause QT interval prolongation.

Table 5 summarizes the effects of 7 and 8 on hemodynamics and electrocardiographic intervals in anesthetized

Table 4. Effect of **8** on Thrombus Weight, aPTT, and Plasma Concentration in the Rat DVT Model

compd	dose/route (mg/kg)	mean thrombus weight (mg/100 g body weight \pm SEM)	decrease in thrombus weight vs vehicle (%)	aPTT	plasma concentration (μ M)
vehicle		21.8 \pm 0.4 (4) ^a		ND ^b	
argatroban	1.0, iv	1.7 \pm 0.3 (5)	92	56 \pm 7	ND
8	0.1, iv	24.7 \pm 3.0 (3)	0	35	0.31 \pm 0.21
	0.3, iv	7.5 \pm 2.4 (5)	66	46 \pm 8	0.54 \pm 0.07
	1.0, iv	0.5 \pm 0.5 (3)	98	49 \pm 8	0.80 \pm 0.06
8	10.0, po	23.0 \pm 1.8 (5)	0	33 \pm 3	0.10 \pm 0.05
	30.0, po	2.9 \pm 0.6 (6)	87	41 \pm 6	0.76 \pm 0.20
	50.0, po	1.3 \pm 0.2 (3)	94	39 \pm 6	0.73 \pm 0.10

^aNumber of animals in parentheses. ^bND, not determined.

Table 5. Effects of **7** and **8** on Hemodynamics and ECG Intervals in Anesthetized Guinea Pigs

		baseline	0.1 mg/kg	0.3 mg/kg	1 mg/kg	3 mg/kg	10 mg/kg
MAP ^a (mm Hg)	8	51 \pm 4	4 \pm 2	5 \pm 2	5 \pm 2	2 \pm 2	-12 \pm 9
	7		0	-5	-10	-15	-21
heart rate (beats/min)	vehicle	47 \pm 12	3 \pm 5	-2 \pm 9	-2 \pm 6	-3 \pm 3	-2 \pm 4
	8	219 \pm 6	0 \pm 1	2 \pm 2	1 \pm 1	-2 \pm 1	-11 \pm 2
QT (ms)	7		-5	-9	-12	-17	-21
	vehicle	242 \pm 12	-1 \pm 2	-4 \pm 6	-2 \pm 7	-4 \pm 5	-6 \pm 5
QTc (ms)	8	176 \pm 3	1 \pm 1	2 \pm 2	2 \pm 1	5 \pm 1	9 \pm 1
	7		4	9	11	14	21
PR (ms)	vehicle	175 \pm 18	2 \pm 1	2 \pm 2	3 \pm 2	6 \pm 3	8 \pm 4
	8	336 \pm 4	1 \pm 0	2 \pm 1	3 \pm 1	3 \pm 2	2 \pm 1
QRS (ms)	7		4	4	5	5	10
	vehicle	353 \pm 9	-3 \pm 5	0 \pm 9	2 \pm 9	2 \pm 8	4 \pm 7
PR (ms)	8	72 \pm 3	2 \pm 2	7 \pm 5	7 \pm 3	6 \pm 5	4 \pm 7
	7		2	1	6	8	13
QRS (ms)	vehicle	68 \pm 2	3 \pm 3	4 \pm 2	2 \pm 2	1 \pm 2	0 \pm 2
	8	27 \pm 4	0 \pm 0	0 \pm 0	-2 \pm 1	-1 \pm 2	0 \pm 3
QRS (ms)	7		3	2	2	3	6
	vehicle	36 \pm 1	-2 \pm 3	-3 \pm 3	-4 \pm 3	-5 \pm 3	-4 \pm 3

^aMean arterial pressure.

guinea pigs at doses of 0.1, 0.3, 1, 3, and 10 mg/kg. At 10 mg/kg iv, **7** increased the QT interval 21% from baseline, and QTc, PR, and QRS intervals were lengthened by 10, 13, and 6%, respectively. Compound **8** had no significant effects on mean arterial pressure through 10 mg/kg (the apparent decrease was due to nondose-dependent blood pressure decreases in one animal) and no effect on heart rate except for a moderate decrease at 10 mg/kg. QT interval, QTc, PR interval, and QRS duration were not significantly affected by **8** at any dose evaluated. Furthermore, at concentrations up to 10 μ M, **8** had no chronotropic or inotropic effects in the isolated right atrium of the guinea pig. Therefore, **8** was deemed to have the more favorable profile and was chosen for continued in vivo assessment.

Despite the slightly increased potency of **7** in vitro [$2 \times$ aPTT = 342 nM vs 510 nM for **8** (Table 3)], the more favorable hERG channel binding value (25% inhibition at 10 μ M vs 50% inhibition at 10 μ M for **8**), and the lower level of human plasma protein binding (49 vs 67% for **8**), **7** compared less favorably to **8** in other respects. As mentioned above, the rat and dog PK parameters of **8** were generally superior to those of **7** with the exception of the $t_{1/2}$ in dogs.

Compound **8** was studied for hemodynamic and electrophysiological effects after oral administration (20 mg/kg) in conscious dogs. Relative to solvent, **8** had no statistically significant effect on heart rate, systolic blood pressure, pressure rate product, cardiac output, stroke volume, the duration of the PQ, QRS, QT, QTcB, QTcF, and QTcVdW intervals, QT dispersion, or on ECG morphology. It tended to decrease diastolic blood pressure (peak effect -20% vs

baseline at 165 min) and systemic vascular resistance (peak effect -26% vs baseline at 75 min) and increase cardiac contractility (LV dp/dt max, LV dp/dt max/pressure) and relaxation (LV dp/dt min).

Target Selectivity for 8. Compound **8** was tested against a panel of 50 receptors and ion channels (Cerep International, France) and did not inhibit paradigm compound binding to any of the receptors by more than 26% at a concentration of 1 μ M. Receptors that demonstrated inhibition > 10% at 1 μ M (AT₁, H₁central, MC₄, NK₂, and κ) and all ion channels were reassessed at 10 μ M. Even at the higher concentration, **8** inhibited paradigm compound binding to only one receptor (L-type Ca²⁺ channel) more than 29%.

Human Clinical Studies. On the basis of these noteworthy preclinical data, **8** was advanced into phase 1 safety and biomarker assessment trials in humans. A double-blind, randomized, placebo-controlled study was conducted to evaluate the safety, tolerability, pharmacokinetics, and pharmacodynamics of single oral doses of **8** (solution formulation) in healthy male volunteers. Eight cohorts of subjects were included. In each cohort, six subjects were randomized to receive a single oral dose of **8** (4, 12, 36, 100, 200, 300, 400, or 500 mg), and two subjects were randomized to receive placebo. Ascending doses of **8** were administered to each cohort. Subjects received a single oral dose of **8** as a solution or matching placebo on the morning of day 1 with 200 mL of water. All subjects had fasted for at least 10 h prior to dose administration. Venous blood samples (5 mL) were collected predose (within 60 min prior to dosing) and at 0.5, 1, 1.5, 2, 2.5, 3, 4, 6, 8, 12, 24, and 48 h postdosing for

determination of plasma concentrations of **8**. The pharmacodynamic parameters assessed in this study focused on

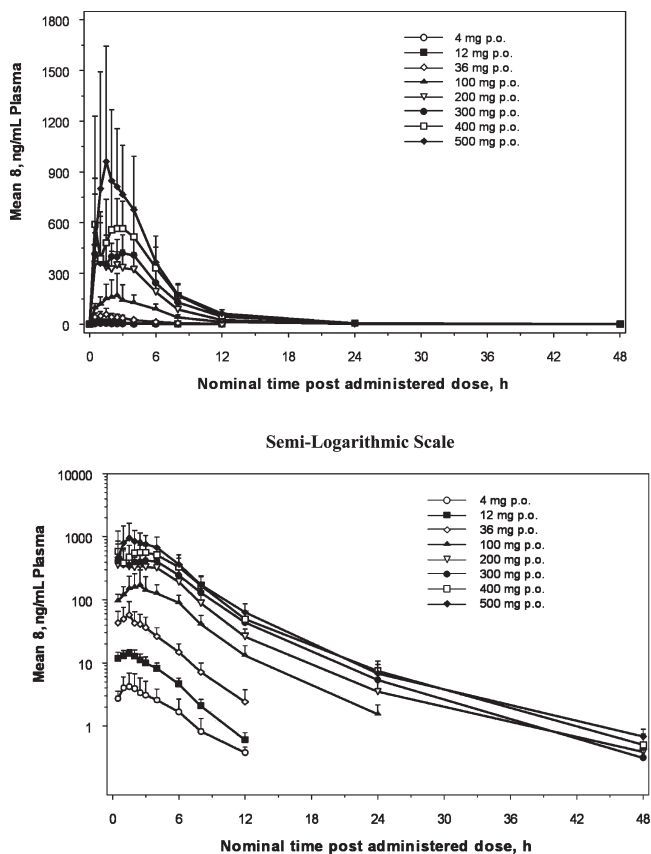


Figure 5. Mean plasma concentration–time profiles of **8** in healthy human volunteers.

evaluating the effect of **8** on coagulation and hemostasis. Evaluated were the following parameters: aPTT, expressed in seconds and as a ratio relative to individual subject baseline (−1 h) values; prothrombin time (PT), expressed in seconds and International Normalized Ratio; ecarin clotting time (ECT), expressed in seconds; and activated clotting time (ACT), expressed in seconds.

Compound **8** was rapidly absorbed into the plasma: the median t_{max} ranged from 1.25 to 2.50 h (Figure 5; linear and semilogarithmic scales shown). However, subjects generally showed more than one peak in the pharmacokinetic profile. Multiple peaks were also observed in rat studies after oral dosing and are hypothesized to be due to enterohepatic recirculation, supported by results of an additional rat biliary excretion study (data not shown).

The mean terminal half-life was consistent across the dose range and ranged from 3.85 to 5.57 h; however, due to minimal sampling times in the 12–48 h period, these data should be interpreted with caution. The majority of **8** was removed from the plasma within 12 h postdosing: Concentrations at 12 h postdose were <17% of the C_{max} . The mean apparent volume of distribution (V/F) ranged from 530 to 806 L, and the mean apparent clearance (CL/F) varied from 85.3 to 109 L/h across the 100–500 mg dose range.

As compared with placebo, mean aPTT values increased in subjects receiving **8** at doses of 100 mg or higher (Figure 6). Mean aPTT values peaked between 0.5 and 4 h postdosing (around the same time maximum plasma concentrations were observed) and returned to baseline at around 24 h postdose. The overall effect of **8** on aPTT increased with higher doses, with the greatest effect seen in the 500 mg dose group. A similar pattern of results was observed for the other ex vivo clotting parameters (PT, ACT, and ECT).

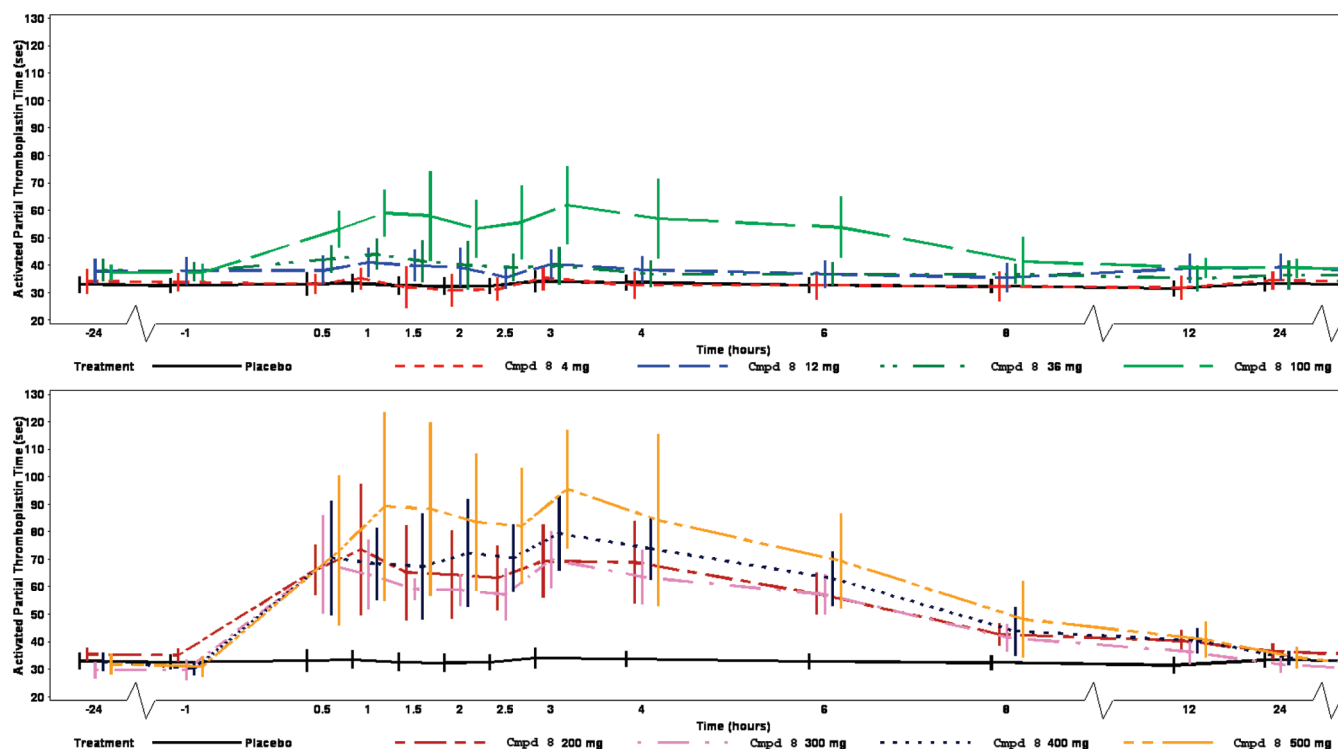


Figure 6. Mean plasma aPTT–time profiles as a function of **8** in healthy human volunteers.

Conclusion

We have explored a series of potent nonpeptidic pyrazinone-based thrombin inhibitors featuring a P1 oxyguanidine moiety, which led to **8** as a promising clinical candidate. This compound exhibited good binding affinity, notable results in a variety of in vitro screening assays, greatly improved PK as compared to thrombin inhibitors with highly basic guanidine/amidine P1 groups, and impressive efficacy in several in vivo thrombosis models, such as ECAT, AV shunt, and DVT. Given the favorable preclinical efficacy and safety profiles for **8**, it was advanced into human clinical studies. The initial results from the successful completion of phase I clinical safety, tolerability, PK, and pharmacodynamic studies of **8** were promising.

Experimental Section

Chemistry. Reagents and solvents were obtained from commercial suppliers and used without further purification. Flash chromatography was performed using Fisher Chemical Silica Gel Sorbent (230–400 mesh, grade 60). ¹H NMR spectra were recorded on a Bruker B-ACS-120 (400 MHz) spectrophotometer at room temperature. Chemical shifts are given in ppm (δ), coupling constants (J) are in hertz (Hz), and signals are designated as follows: (s) singlet, (d) doublet, (t) triplet, (q) quartet, (m) multiplet, (br s) broad singlet, (br t) broad triplet, (br m) broad multiplet, (dd) doublet of doublet, (dt) doublet of triplet, (td) triplet of doublet, (dq) doublet of quartet, (tm) triplet of multiplet, (ddd) doublet of doublet of doublet, (ddt) doublet of doublet of triplet, and (dddd) doublet of doublet of doublet of doublet. LC-MS was performed on a system consisting of an electrospray source on a Finnigan LCQ ion trap mass spectrometer, a SEDEX 75C evaporative light scattering detector, a Shimadzu LC-10ADvp binary gradient pumping system, a Gilson 215 configured as an autosampler, and a Princeton Chromatography HTS HPLC column (5 μ m, 50 mm \times 3.0 mm). Accurate mass measurements were performed using either of two methods: (1) A Micromass (Manchester, United Kingdom) Autospec E OA-TOF high-resolution magnetic sector mass spectrometer was tuned to a resolution of > 5000 using the 5% valley definition. The ions were produced in a fast atom bombardment (FAB) ion source at an accelerating voltage of 8 kV. Linear voltage scans at 33 Da/s were collected to include the protonated sample ion and two polyethylene glycol (PEG) or PEG monomethyl ether ions, which were used as internal reference standards. The molecular mass was calculated using a linear extrapolation method. Reported mass values are averages over 100 s. (2) Positive ion electrospray (ESI) high-resolution mass spectrometry was carried out with a Micromass Q-ToF API US hybrid quadrupole/time-of-flight mass spectrometer. The mass spectrometer was externally calibrated using cesium iodide. PEG 400 was added to the samples as an internal calibrant. The purities of some key target compounds were determined on a Varian HPLC system equipped with two Varian PrepStar delivery pumps (model 218) and a Varian UV-vis detector (model 345). The HPLC method used was as follows: column, PrincetonSPHER-100 Phenyl, 4.6 mm \times 150 mm, 5 μ m; column temperature, ambient; flow rate, 1.0 mL/min; gradient, 20% acetonitrile (0.01% TFA and 0.2% formic acid) in water (0.01% TFA and 0.2% formic acid) to 80% acetonitrile (0.01% TFA and 0.2% formic acid) in water (0.01% TFA and 0.2% formic acid) in 30 min. All of the final compounds had 95% or greater purity.

***N*-[2-(Benzyloxycarbonylamino)ethoxy]phthalimide (1).** To a solution of benzyl *N*-(2-hydroxyethyl)carbamate (5.9 g, 30 mmol), *N*-hydroxyphthalimide (4.9 g, 30 mmol), and triphenylphosphine (7.9 g, 30 mmol) in tetrahydrofuran (100 mL) was added diethyl azodicarboxylate (5.2 g, 30 mmol). The reaction mixture was stirred at room temperature overnight. Ethyl

acetate (200 mL) was added, washed with saturated NaHCO₃ (2 \times 100 mL) and brine (100 mL), dried over Na₂SO₄, and filtered. After the filtrate was evaporated, the residue was purified by flash column chromatography (methylene chloride/ethyl acetate, 1:0 to 96:4, v/v) to give compound **1** as a white solid (9.3 g, 91%). ¹H NMR (CDCl₃): δ 7.84 (m, 2H), 7.78 (m, 2H), 7.37 (m, 5H), 5.97 (br s, 1H), 5.14 (s, 2H), 4.27 (t, J = 4.9 Hz, 2H), 3.51 (q, J = 5.2 Hz, 2H).

2-(Benzyloxycarbonylamino)ethoxyamine (2). To a solution of **1** (1.4 g, 4.0 mmol) in ethanol (20 mL) and tetrahydrofuran (20 mL) was added 40% methanolamine (2.0 mL, 25 mmol), and the mixture stirred at room temperature for 1 h. After the solvent was evaporated, the residue was purified by flash column chromatography (hexane/ethyl acetate, 3:1 to 0:1, v/v) to give **2** as a white solid (800 mg, 95%). ¹H NMR (CDCl₃): δ 7.36 (m, 5H), 5.47 (br s, 2H), 5.21 (br s, 1H), 5.10 (s, 2H), 3.72 (t, J = 5.0 Hz, 2H), 3.44 (q, J = 5.0 Hz, 2H).

[*N,N'*-Di-(*tert*-butoxycarbonyl)]-2-(benzyloxycarbonylamino)-ethoxyguanidine (3). To a solution of **2** (0.78 g, 3.7 mmol) in *N,N*-dimethylformamide (20 mL) was added [*N,N'*-di-(*tert*-butoxycarbonyl)]amidinopyrazole (1.3 g, 4.0 mmol). The mixture was stirred at room temperature overnight, and the solvent was evaporated under high vacuum. The residue was purified by flash column chromatography (methylene chloride/ethyl acetate, 1:0 to 95:5, v/v) to give **3** as a colorless oil (1.55 g, 93%). ¹H NMR (CDCl₃): δ 9.08 (s, 1H), 7.33 (m, 5H), 6.21 (br s, 1H), 5.21 (br s, 1H), 5.11 (s, 2H), 4.12 (t, J = 4.8 Hz, 2H), 3.54 (q, J = 4.9 Hz, 2H), 1.49 (s, 9H), 1.46 (s, 9H).

[*N,N'*-Di-(*tert*-butoxycarbonyl)]-2-aminoethoxyguanidine (4). A mixture of **4** (730 mg, 1.5 mmol), as prepared in the preceding step, 10% palladium on carbon (70 mg) in ethanol (20 mL), and tetrahydrofuran (20 mL) was hydrogenated under hydrogen (balloon) for 30 min. The catalysts were removed by filtration through diatomaceous earth, and the filtrate was concentrated in vacuo. The residue was purified on a 10 g Waters Sep-Pak (methylene chloride/methanol saturated with ammonia, 95:5, v/v) to give the title compound as a colorless oil (290 mg, 61%). ¹H NMR (CDCl₃): δ 9.08 (br s, 1H), 4.08 (t, J = 5.2 Hz, 2H), 2.99 (q, J = 5.1 Hz, 2H), 1.50 (s, 9H), 1.48 (s, 9H).

Representative Procedure for the Synthesis of 1-{*N*-[2-(Amidinoaminoxy)ethyl]amino}carbonylmethyl-6-substituted-3-alkylpyrazinones (7–18). Synthesis of 7. Step A: [6-Cyano-3-(2,2-difluoro-2-phenyl-ethylamino)-2-oxo-2*H*-pyrazin-1-yl]acetic Acid Ethyl Ester. Compound **5** (0.20 g, 0.83 mmol) was dissolved in toluene (5 mL), treated with 2,2-difluoro-2-phenylethylamine (0.80 g, 5.1 mmol), and heated to 60 °C for 3 h. The reaction was concentrated to dryness, and the residue was dissolved in dichloromethane, washed with 5% aqueous HCl, saturated NaHCO₃, and brine, dried over Na₂SO₄, and filtered. The filtrate was concentrated to dryness, adsorbed onto silica gel, poured onto a 7 cm \times 3 cm pad of silica gel, and eluted with ethyl acetate/dichloromethane, 0:1 to 1:9, v/v. The fractions were concentrated in vacuo giving [6-cyano-3-(2,2-difluoro-2-phenyl-ethylamino)-2-oxo-2*H*-pyrazin-1-yl]acetic acid ethyl ester as a light orange solid (0.29 g, 95%). ¹H NMR (CDCl₃): δ 7.53 (m, 2H), 7.46 (m, 3H), 7.38 (s, 1H), 6.95 (br m, 1H), 4.79 (s, 2H), 4.29 (q, 2H, J = 7.1 Hz), 4.16 (td, 2H, J = 6.5 Hz, 14.2 Hz), 1.32 (t, 3H, J = 7.1 Hz).

Step B: [6-Cyano-3-(2,2-difluoro-2-phenyl-ethylamino)-2-oxo-2*H*-pyrazin-1-yl]acetic Acid. The product of step A (0.28 g, 0.77 mmol) was dissolved in 1,4-dioxane (10 mL) and treated with 1 N NaOH (4 mL) at ambient temperature. After it was stirred for 1.5 h, the reaction was concentrated to dryness, dissolved in hot water (10 mL), acidified with 10% aqueous HCl, and cooled to ambient temperature, and the precipitate was filtered. The solids were washed with water, dissolved in tetrahydrofuran, and filtered, and the filtrate was concentrated in vacuo giving [6-cyano-3-(2,2-difluoro-2-phenyl-ethylamino)-2-oxo-2*H*-pyrazin-1-yl]acetic acid as a gummy red-orange solid (0.27 g, 100% for the hydrate). ¹H NMR (DMSO-*d*₆): δ 8.64 (t, 1H,

$J = 6.6$ Hz), 7.62 (s, 1H), 7.53 (m, 5H), 4.72 (s, 2H), 4.14 (td, 2H, $J = 6.6$ Hz, 15 Hz). MS m/z [MH^+] 334.9.

Step C: 1- $\{N$ -[2-(N' , N'' -Bis(*tert*-butoxycarbonyl)amidinoaminoxy)ethyl]amino}carbonylmethyl-6-cyano-3-[2,2-difluoro-2-phenylethylamino]pyrazinone. The product of step B (0.27 g, 0.77 mmol) was dissolved in anhydrous N,N -dimethylformamide (10 mL) and treated with **4**, Castro's reagent (0.42 g, 0.95 mmol), and triethylamine (0.30 mL, 2.2 mmol). After it was stirred at room temperature for 18 h, the reaction was concentrated to an oil, dissolved in dichloromethane, washed with 10% aqueous citric acid, water, and brine, dried over Na_2SO_4 , and filtered. The filtrate was concentrated to dryness, the crude product was purified by flash column chromatography on silica gel with ethyl acetate/hexanes, 1:1 to 2:1, v/v, and the fractions were concentrated in vacuo giving 1- $\{N$ -[2-(N' , N'' -bis(*tert*-butoxycarbonyl)amidinoaminoxy)ethyl]amino}carbonylmethyl-6-cyano-3-[2,2-difluoro-2-phenylethylamino]pyrazinone as a pale yellow solid (0.35 g, 71%). 1H NMR ($CDCl_3$): δ 9.19 (br s, 1H), 8.78 (br s, 1H), 7.55 (m, 2H), 7.48 (m, 3H), 7.37 (s, 1H), 6.94 (t, 1H, $J = 6.3$ Hz), 4.88 (s, 2H), 4.15 (m, 4H), 3.66 (m, 2H), 1.54 (s, 9H), 1.51 (s, 9H). MS m/z [MH^+] 634.8.

Step D: 1- $\{N$ -[2-(Amidinoaminoxy)ethyl]amino}carbonylmethyl-6-cyano-3-[2,2-difluoro-2-phenylethylamino]pyrazinone Dihydrochloride (**7**). The product of step C (0.34 g, 0.54 mmol) was dissolved in dichloromethane (10 mL), treated with trifluoroacetic acid (5 mL), and stirred at ambient temperature for 8 h. The reaction was concentrated to dryness, the crude product was purified by flash column chromatography on silica gel with methanol/dichloromethane saturated with ammonia gas, 85:15, v/v, and the fractions were concentrated in vacuo. The column fractions were treated with 4 N HCl in ethanol, concentrated under high vacuum, and filtered, giving **7** as a white solid (0.19 g, 82%). 1H NMR ($DMSO-d_6$): δ 8.50 (br t, 1H, $J = 6.1$ Hz), 8.41 (t, 1H, $J = 5.5$ Hz), 7.57 (s, 1H), 7.52 (m, 5H), 5.13 (br s, 2H), 4.62 (s, 2H), 4.40 (br s, 2H), 4.13 (td, 2H, $J = 5.5$ Hz, 15 Hz), 3.63 (t, 2H, $J = 5.6$ Hz), 3.30 (q, 2H, $J = 5.6$ Hz). MS m/z [MH^+] 435.1. Anal. ($C_{18}H_{20}F_2N_8O_3 \cdot 2HCl \cdot 0.1H_2O \cdot 0.17CH_3N$) C, H, N.

1- $\{N$ -[2-(Amidinoaminoxy)ethyl]amino}carbonylmethyl-6-methyl-3-[2,2-difluoro-2-phenylethylamino]pyrazinone Dihydrochloride (**8**). Yield, 37%; mp 211–214 °C. 1H NMR (400 MHz, $DMSO-d_6$): δ 10.89 (s, 1H), 8.46 (t, $J = 5.5$ Hz, 1H), 7.69 (br s, 4H), 7.53 (m, 2H), 7.50 (m, 3H), 6.84 (t, $J = 6.5$ Hz, 1H), 6.64 (s, 1H), 4.62 (s, 2H), 4.06 (dt, $J = 6.5$, 14.4 Hz, 2H), 3.81 (t, $J = 5.4$ Hz, 2H), 3.38 (m, 2H), 2.06 (s, 3H). MS m/z [MH^+] 424.4. Anal. ($C_{18}H_{23}F_2N_8O_3 \cdot 2HCl \cdot 0.15H_2O$) C, H, N.

1- $\{N$ -[2-(Amidinoaminoxy)ethyl]amino}carbonylmethyl-6-methyl-3-(4-fluorophenethylamino)pyrazinone Bis-trifluoroacetic Acid Salt (**9**). 1H NMR ($DMSO-d_6$): δ 10.97 (s, 1H), 8.45 (t, $J = 5.6$ Hz, 1H), 7.74 (br s, 4H), 7.26 (m, 2H), 7.15 (t, $J = 8.8$ Hz, 2H), 6.68 (s, 1H), 4.61 (s, 2H), 3.81 (t, $J = 5.4$ Hz, 2H), 3.39 (m, 4H), 2.85 (t, $J = 7.3$ Hz, 2H), 2.07 (s, 3H). MS m/z [MH^+] 406.6. HPLC $t_R = 5.06$ min, >98% pure.

1- $\{N$ -[2-(Amidinoaminoxy)ethyl]amino}carbonylmethyl-6-methyl-3-(2-[3,4-difluorophenyl]ethylamino)pyrazinone Dihydrochloride (**10**). 1H NMR ($DMSO-d_6$): δ 11.05 (s, 1H), 8.63 (t, 1H, $J = 5.5$ Hz), 7.74 (br s, 4H), 7.46 (t, 1H, $J = 10$ Hz), 7.36 (dt, 1H, $J = 10.9$ Hz, 8.5 Hz), 7.15 (m, 1H), 6.70 (s, 1H), 4.66 (s, 2H), 3.82 (t, 2H, $J = 5.4$ Hz), 3.66 (m, 2H), 3.38 (m, 2H), 2.91 (t, 2H, $J = 7.4$ Hz), 2.13 (s, 3H). MS m/z [MH^+] 424.4. HPLC $t_R = 5.33$ min, >98% pure.

1- $\{N$ -[2-(Amidinoaminoxy)ethyl]amino}carbonylmethyl-6-methyl-3-(2-[2,4-difluorophenyl]ethylamino)pyrazinone Bis-trifluoroacetic Acid Salt (**11**). 1H NMR ($DMSO-d_6$): δ 11.03 (s, 1H), 8.46 (t, $J = 5.6$ Hz, 1H), 7.77 (br s, 4H), 7.34 (q, $J = 7.8$ Hz, 1H), 7.18 (t, $J = 9.5$ Hz, 1H), 7.03 (t, $J = 8.0$ Hz, 1H), 6.67 (s, 1H), 4.62 (s, 2H), 3.81 (t, $J = 5.4$ Hz, 2H), 3.51 (m, 2H), 3.39 (t, $J = 5.5$ Hz, 2H), 2.89 (t, $J = 7.1$ Hz, 2H), 2.08 (s, 3H). MS m/z [MH^+] 424.4. HPLC $t_R = 5.81$ min, >98% pure.

1- $\{N$ -[2-(Amidinoaminoxy)ethyl]amino}carbonylmethyl-6-methyl-3-(2-[4-trifluoromethylphenyl]ethylamino)pyrazinone Bis-trifluoroacetic Acid Salt (**12**). 1H NMR ($DMSO-d_6$): δ 10.98 (s, 1H), 8.45 (t, 1H, $J = 5.5$ Hz), 7.74 (br s, 4H), 7.66 (d, 2H, $J = 8.1$ Hz), 7.47 (d, 2H, $J = 8.0$ Hz), 6.68 (s, 1H), 4.62 (s, 2H), 3.81 (t, 2H, $J = 5.4$ Hz), 3.50 (m, 2H), 3.38 (q, 2H, $J = 5.4$ Hz), 2.97 (t, 2H, $J = 7$ Hz), 2.08 (s, 3H). MS m/z [MH^+] 456.2. HPLC $t_R = 6.32$ min, >98% pure.

1- $\{N$ -[2-(Amidinoaminoxy)ethyl]amino}carbonylmethyl-6-methyl-3-(4-methoxyphenethylamino)pyrazinone Bis-trifluoroacetic Acid Salt (**13**). 1H NMR ($DMSO-d_6$): δ 10.88 (s, 1H), 8.42 (t, $J = 5.5$ Hz, 1H), 7.68 (br s, 4H), 7.15 (d, $J = 8.6$ Hz, 2H), 6.85 (d, $J = 8.7$ Hz, 2H), 6.67 (s, 1H), 4.61 (s, 2H), 3.81 (t, $J = 5.3$ Hz, 2H), 3.72 (s, 3H), 3.50 (m, 2H), 3.38 (m, 2H), 2.79 (t, $J = 6.9$ Hz, 2H), 2.07 (s, 3H). MS m/z [MH^+] 418.3. Anal. ($C_{19}H_{27}N_7O_4 \cdot 2C_2HF_3O_2 \cdot 0.75H_2O$) C, H, N.

1- $\{N$ -[2-(Amidinoaminoxy)ethyl]amino}carbonylmethyl-6-methyl-3-(3,4-dimethoxyphenethylamino)pyrazinone Bis-trifluoroacetic Acid Salt (**14**). 1H NMR ($DMSO-d_6$): δ 10.95 (s, 1H), 8.44 (t, $J = 5.6$ Hz, 1H), 7.72 (br s, 4H), 6.85 (t, $J = 8.1$ Hz, 2H), 6.73 (d, $J = 8.1$ Hz, 1H), 6.67 (s, 1H), 4.61 (s, 2H), 3.81 (t, $J = 5.3$ Hz, 2H), 3.73 (s, 3H), 3.71 (s, 3H), 3.39 (m, 4H), 2.79 (t, $J = 7.2$ Hz, 2H), 2.07 (s, 3H). MS m/z [MH^+] 448.2. HPLC $t_R = 4.84$ min, >98% pure.

1- $\{N$ -[2-(Amidinoaminoxy)ethyl]amino}carbonylmethyl-6-methyl-3-(4-ethylphenethylamino)pyrazinone Bis-trifluoroacetic Acid Salt (**15**). 1H NMR ($DMSO-d_6$): δ 10.97 (s, 1H), 8.44 (t, $J = 5.6$ Hz, 1H), 7.73 (br s, 4H), 7.14 (s, 4H), 6.67 (s, 1H), 4.61 (s, 2H), 3.81 (t, $J = 5.2$ Hz, 2H), 3.39 (m, 4H), 2.82 (t, $J = 7.5$ Hz, 2H), 2.56 (q, $J = 7.6$ Hz, 2H), 2.07 (s, 3H), 1.16 (t, $J = 7.5$ Hz, 3H). MS m/z [MH^+] 416.2. Anal. ($C_{20}H_{29}N_7O_3 \cdot 2C_2HF_3O_2 \cdot 0.5H_2O$) C, H, N.

1- $\{N$ -[2-(Amidinoaminoxy)ethyl]amino}carbonylmethyl-6-methyl-3-(2-[5-indanyl]ethylamino)pyrazinone Dihydrochloride (**16**). 1H NMR ($DMSO-d_6$): δ 11.13 (s, 1H), 8.71 (t, 1H, $J = 5.5$ Hz), 7.78 (br s, 4H), 7.19 (s, 1H), 7.14 (d, 1H, $J = 7.7$ Hz), 7.07 (m, 1H), 6.70 (s, 1H), 4.67 (s, 2H), 3.82 (t, 2H, $J = 5.3$ Hz), 3.65 (m, 2H), 2.84 (m, 6H), 2.13 (s, 3H), 1.99 (pentet, 2H, $J = 7.4$ Hz). MS m/z [MH^+] 428.3. HPLC $t_R = 5.20$ min, >98% pure.

1- $\{N$ -[2-(Amidinoaminoxy)ethyl]amino}carbonylmethyl-6-methyl-3-[2-(1-naphthalene)ethyl]aminopyrazinone Dihydrochloride (**17**). 1H NMR (400 MHz, $DMSO-d_6$): δ 11.1 (s, 1H), 8.71 (t, 1H, $J = 5.3$ Hz), 8.26 (d, 1H, $J = 8.2$ Hz), 7.94 (d, 1H, $J = 8.1$ Hz), 7.83 (d, 1H, $J = 8.2$ Hz), 7.78 (br s, 4H), 7.56 (m, 3H), 7.46 (t, 1H, $J = 7.5$ Hz), 6.73 (s, 1H), 4.69 (s, 2H), 3.80 (m, 4H), 3.42 (m, 4H), 2.14 (s, 3H). MS m/z [MH^+] 438.2. Anal. ($C_{22}H_{27}N_7O_3 \cdot 2HCl \cdot 0.75H_2O$) C, H, N.

1- $\{N$ -[2-(Amidinoaminoxy)ethyl]amino}carbonylmethyl-6-methyl-3-(2,2-diphenylethylamino)pyrazinone Bis-trifluoroacetic Acid Salt (**18**). 1H NMR (300 MHz, $DMSO-d_6$): δ 10.92 (s, 1H), 8.44 (t, $J = 5.6$ Hz, 1H), 7.71 (br s, 4H), 7.11 (s, 4H), 6.67 (s, 1H), 4.61 (s, 2H), 3.81 (t, $J = 5.4$ Hz, 2H), 3.50 (m, 2H), 3.38 (m, 2H), 2.81 (t, $J = 6.9$ Hz, 2H), 2.27 (s, 3H), 2.07 (s, 3H). MS m/z [MH^+] 402.1. Anal. ($C_{24}H_{29}N_7O_3 \cdot 2C_2HF_3O_2 \cdot 1.0H_2O$) C, H, N.

[6-Chloro-3-(2,2-difluoro-2-phenyl-ethylamino)-2-oxo-2H-pyrazin-1-yl]acetic Acid (**20**). Compound **19** (0.78 g, 3.0 mmol) was dissolved in toluene (10 mL), treated with 2,2-difluoro-2-phenylethylamine (1.0 g, 6.4 mmol), heated to reflux for 12 h, and then stirred at ambient temperature for 3 days. The reaction was concentrated to dryness in vacuo, the crude product was purified by flash column chromatography on silica gel with hexanes/ethyl acetate, 1:1, v/v as eluant, and the column fractions were concentrated in vacuo giving [3-(2,2-difluoro-2-phenyl-ethylamino)-2-oxo-2H-pyrazin-1-yl]acetic acid ethyl ester as a pale orange solid (0.75 g, 75%). 1H NMR (400 MHz, $CDCl_3$): δ 7.56 (m, 2H), 7.45 (m, 3H), 6.83 (d, 1H, $J = 4.7$ Hz), 6.42 (d, 1H, $J = 4.7$ Hz), 6.36 (m, 1H), 4.57 (s, 2H), 4.26 (q, 2H, $J = 7$ Hz), 4.13 (td, 2H, $J = 6$ Hz, 14 Hz), 1.31 (t, 3H, $J = 7$ Hz).

Next, a solution of [3-(2,2-difluoro-2-phenyl-ethylamino)-2-oxo-2H-pyrazin-1-yl]acetic acid ethyl ester (0.75 g, 2.2 mmol) and *N*-chlorosuccinimide (0.30 g, 2.3 mmol) in 1,2-dichloroethane (40 mL) was heated to reflux for 2.5 h. After it was cooled to room temperature, the reaction was washed with saturated aqueous NaHCO₃ and brine, dried over Na₂SO₄, and filtered, and the filtrate was concentrated to dryness. The crude product was then adsorbed onto silica gel, poured onto a 3 cm × 6 cm pad of silica gel, eluted with hexanes/ethyl acetate, 3:1 to 2:1, v/v, and the fractions were concentrated in vacuo giving [6-chloro-3-(2,2-difluoro-2-phenyl-ethylamino)-2-oxo-2H-pyrazin-1-yl]acetic acid ethyl ester as a pale orange solid (0.67 g, 81%). ¹H NMR (400 MHz, CDCl₃): δ 7.53 (m, 2H), 7.43 (m, 3H), 6.90 (s, 1H), 6.25 (br t, 1H, *J* = 5.8 Hz), 4.89 (s, 2H), 4.26 (q, 2H, *J* = 7 Hz), 4.09 (td, 2H, *J* = 6 Hz, 14 Hz), 1.30 (t, 3H, *J* = 7.2 Hz). MS *m/z* [MH⁺] 352.0.

[6-Chloro-3-(2,2-difluoro-2-phenyl-ethylamino)-2-oxo-2H-pyrazin-1-yl]acetic acid ethyl ester (0.67 g, 1.8 mmol) was then dissolved in 1,4-dioxane (24 mL) and treated with 1 N aqueous NaOH (8.0 mL, 8.0 mmol). After it was stirred at ambient temperature for 18 h, the reaction was concentrated to dryness, dissolved in water, and treated with 10% aqueous HCl to pH 4, and the white precipitate was filtered, washed thrice with water and once with hexane, and dried in vacuo giving **20** as a white solid (0.56 g, 90%). ¹H NMR (400 MHz, DMSO-*d*₆): δ 7.50 (m, 5H), 6.95 (s, 1H), 4.79 (s, 2H), 4.06 (td, 2H, *J* = 6.5 Hz, 15 Hz).

1-[*N*-[2-(Amidinoaminoxy)ethyl]amino]carbonylmethyl-6-chloro-3-[2,2-difluoro-2-phenylethylamino]pyrazinone Dihydrochloride (21). Compound **20** (0.56 g, 1.6 mmol) was dissolved in anhydrous *N,N*-dimethylformamide (25 mL) and treated with [*N,N*-di(*tert*-butoxycarbonyl)]-2-aminoethoxyguanidine (0.64 g, 2.0 mmol), Castro's reagent (0.89 g, 2.0 mmol), and triethylamine (1.0 mL, 7.2 mmol). After it was stirred at ambient temperature for 3 days, the reaction was concentrated to dryness in vacuo, the residue was dissolved in dichloromethane, washed with 10% aqueous citric acid, water, saturated aqueous NaHCO₃, and brine, dried over Na₂SO₄, and filtered, and the filtrate was concentrated in vacuo. The crude product was adsorbed onto silica gel, poured onto a 7 cm × 3 cm pad of silica gel, and eluted with hexanes/ethyl acetate, 2:1 to 0:1, v/v, and the fractions were concentrated in vacuo giving 1-[*N*-[2-(*N',N''*-bis(*tert*-butoxycarbonyl)amidinoaminoxy)ethyl]amino]carbonylmethyl-6-chloro-3-[2,2-difluoro-2-phenylethylamino]pyrazinone as a light yellow solid (0.91 g, 86%). ¹H NMR (400 MHz, CDCl₃): δ 9.15 (s, 1H), 8.55 (br t, 1H, *J* = 5 Hz), 7.53 (m, 3H [Aryl + NH]), 7.43 (m, 3H), 6.88 (s, 1H), 6.25 (t, 1H, *J* = 6.4 Hz), 4.96 (s, 2H), 4.11 (m, 4H), 3.63 (dd, 2H, *J* = 4.9 Hz, 8.5 Hz), 1.51 (s, 9H), 1.49 (s, 9H).

1-[*N*-[2-(*N',N''*-Bis(*tert*-butoxycarbonyl)amidinoaminoxy)ethyl]amino]carbonylmethyl-6-chloro-3-[2,2-difluoro-2-phenylethylamino]pyrazinone (0.91 g, 1.4 mmol) was then dissolved in dichloromethane (10 mL), treated with trifluoroacetic acid (5 mL), and stirred at ambient temperature for 24 h. The reaction was concentrated in vacuo, the residue purified by flash column chromatography on silica gel with methanol/dichloromethane saturated with ammonia gas, 1:9 to 15:85, v/v, and the fractions were concentrated in vacuo. The column fractions were treated with 4 N HCl in ethanol, concentrated under high vacuum, and filtered, giving **21** as a white solid (0.53 g, 85%). ¹H NMR (400 MHz, DMSO-*d*₆): δ 8.32 (m, 1H), 7.52 (m, 5H), 7.40 (t, 1H, *J* = 7 Hz), 6.92 (s, 1H), 5.16 (br m, 1H), 4.72 (s, 2H), 4.42 (br m, 1H), 4.06 (td, 2H, *J* = 6.6 Hz, 15.2 Hz), 3.62 (t, 2H, *J* = 5.5 Hz), 3.28 (q, 2H, *J* = 5.5 Hz). MS *m/z* [MH⁺] 444.1. Anal. (C₁₇H₂₀-ClF₂N₇O₃·2HCl·0.33H₂O) C, H, N.

1-[*N*-[2-(Amidino-*N'*-methylaminoxy)ethyl]amino]carbonylmethyl-6-methyl-3-(2-[4-methylphenyl]ethylamino)pyrazinone Dihydrochloride (22). To a mixture of 1-[*N*-[2-(amidinoaminoxy)ethyl]amino]carbonylmethyl-6-methyl-3-(4-methylphenylethylamino)pyrazinone²⁹ (0.076 g, 0.19 mmol) and sodium bicarbonate (0.53 g, 6.3 mmol) in *N,N*-dimethylformamide (10 mL) was added iodomethane (0.040 mL, 0.64 mmol). After it was stirred for 2 days

at ambient temperature, the solution was concentrated in vacuo, and the residue was treated with pH 1 brine and made basic with solid KOH. The resulting precipitate was filtered, washed with water, and removed from the filter with methanol. The filtrate was concentrated in vacuo, dissolved in methanol/dichloromethane, 1:1, v/v, and filtered. The filtrate was evaporated, and the residue was treated with 2 mL of 4 N HCl in ethanol, dissolved in methanol/dichloromethane, and refiltered, giving the title compound as a yellow solid (0.08 g, 86%). ¹H NMR (400 MHz, DMSO-*d*₆): δ 8.62 (t, 1H, *J* = 5.3 Hz), 7.90 (br s, 3H), 7.18 (d, 2H, *J* = 7.9 Hz), 7.11 (d, 2H, *J* = 7.9 Hz), 6.70 (s, 1H), 4.64 (s, 2H), 3.91 (t, 2H, *J* = 5.2 Hz), 3.39 (q, 2H, *J* = 5.2 Hz), 3.25 (s, 3H), 2.86 (t, 2H, *J* = 7.5 Hz), 2.27 (s, 3H), 2.12 (s, 3H). MS *m/z* [MH⁺] 416.2. HPLC *t*_R = 6.21 min, >98% pure.

Enzymology. All compounds were assessed for inhibitory activity toward thrombin, as well as the key enzymes fXa and trypsin, by kinetic analysis using *p*-nitroaniline chromogenic substrates. The assay buffer employed was 50 mM Hepes, pH 7.5, 200 mM NaCl, and fresh 0.05% *n*-octyl β-D-glucopyranoside. DMSO was present at a final concentration of 4%. In a 96-well low-binding polystyrene plate, 280 μL of substrate in assay buffer was preincubated at 37 °C for 15 min with 10 μL of test compound in DMSO to obtain final test compound concentrations that bracketed the *K*_i. Reactions were initiated by addition of 10 μL of protease, and the increase in absorbance due to proteolytic cleavage of substrate was kinetically monitored at 37 °C and 405 nm with a Molecular Devices Spectramax 340 plate reader. Initial velocities were determined by analysis of the initial linear portion of the reactions. Plots of *v*₀/*v*_i versus inhibitor concentration, where *v*₀ = velocity without inhibitor and *v*_i = inhibited velocity, were fit to a linear regression line, and the IC₅₀ value was determined from the reciprocal of the slope. Alternatively, IC₅₀ values were determined using Graph-Pad Prism software and a four-parameter logistics equation. *K*_i was calculated from the IC₅₀ using the *K*_i factor specific for the assay as: *K*_i = IC₅₀ × *K*_i factor or *K*_i = IC₅₀ × {1/(1 + [S]/*K*_m)}, where S is the substrate concentration in the assay and *K*_m is the Michaelis constant for the substrate.³⁰

The thrombin assay incorporated substrate SucAAPR pNA (Bachem L-1720, [S] = 100 μM final, *K*_m = 320 μM, and *K*_i factor = 0.76). Human α-thrombin (Enzyme Research Laboratories HT1002a) was diluted in assay buffer for a final assay concentration of 1.1 nM. The fXa assay incorporated substrate S-2765 (Diapharma/Chromogenix S-2765, Z-D-Arg-Gly-Arg-pNA·2HCl, [S] = 100 μM final, *K*_m = 260 μM, and *K*_i factor = 0.72). Human fXa (Enzyme Research Laboratories HFXa 1500) was diluted in assay buffer for a final assay concentration of 0.53 nM.

The trypsin assay also incorporated substrate S-2765 ([S] = 60 μM final, *K*_m = 61 μM, and *K*_i factor = 0.50). Human trypsin (Calbiochem 650275) was diluted in assay buffer for 333 pM final concentration. The within-run assay coefficient of variation (CV) was generally <10%; the between-run CV was <20%. The inhibitory capacity of **7** and **8** for other proteases was determined by CEREP protease assay service.

Crystallization, Data Collection, and Structure Determination and Refinement. Human α-thrombin was purchased from Enzyme Research Laboratories and crystallized at 4 °C in a complex with sulfated hirudin 53-65 (Bachem Biosciences) as previously described.³¹ Complexes of thrombin with the hirudin fragment and active site-directed inhibitors were formed by adding inhibitor solutions to standing vapor diffusion drops (2 μL) containing large single crystals of μ-thrombin. Crystals were undamaged by this procedure and were mounted for data collection 4–5 h after the addition of inhibitors. Compound **8** was dissolved in DMSO at a concentration of 200 mM and then diluted to 4 mM in 28% PEG 8000 containing 100 mM phosphate buffer (pH 7.3), 0.15 M NaCl, and 3 mM NaN₃. An aliquot (1 μL) of this solution was added to a drop (2 μL) containing single thrombin crystals to produce a final inhibitor concentration of 1.3 mM.

The crystals were then transferred to a cryoprotectant solution containing 40% PEG 3350, 10 mM CaCl₂, and 100 mM Tris-maleate at a pH of 5.5 and flash frozen by immersion in liquid nitrogen. X-ray diffraction data to a resolution of 2.06 Å were collected on a Bruker AXS Proteum 6000 detector. Diffraction data were indexed, integrated, and scaled using the Proteum Processing Program suite from Bruker AXS. The crystal belongs to the C2 space group, with unit cell parameters $a = 71.1$ Å, $b = 72.0$ Å, $c = 73.41$ Å, and $\beta = 101.06$. The structure was determined by molecular replacement with CNX³² using the PDB³³ coordinates 1QBV as the search model. All model building was done using the computer program CHAIN;³⁴ refinement and map calculations were carried out using CNX.³⁴ The final structure was refined to an Rfactor of 17.8 and Rfree of 22.8.

Platelet Aggregation. PRP concentrate (Biological Specialties, Inc.) was diluted with platelet-poor plasma (PPP) to yield a final plate count per well of 300 000 platelets/ μ L. PPP was obtained by spinning PRP at 3000 rpm for 10 min at 25 °C. H-Gly-Pro-Arg-Pro-NH₂ (GPRP-NH₂, final concentration of 4 mM) was added to the PRP to minimize the effects of fibrinogen. Aggregation was run in a 96-well assay plate with a total volume of 150 μ L (120 μ L of PRP, 15 μ L of inhibitor, and 15 μ L of agonist) in each well.

Animal Studies. All procedures involving the use of animals were performed in accordance with the Guide for the Care and Use of Laboratory Animals (1996) and the Animal Care and Use Committee, Johnson and Johnson Pharmaceutical Research and Development.

In Vitro Coagulation Assays. The plasma concentrations of **7** and **8** needed to produce a 2-fold prolongation of aPTT were determined in human plasma. Fresh whole blood from humans, dogs, and rats was centrifuged to obtain plasma, and the thrombin inhibitors were added to yield concentrations from 0.001 to 100 μ M. After a short stabilization period, the samples were placed in an automated coagulation analyzer (Instrumentation Laboratory ACL100, Beckman Coulter, Miami, FL) to determine clotting times in seconds.

Rat DVT Model. Male Sprague–Dawley Rats (300–450 g) were anesthetized with a mixture of ketamine and xylazine (1 mL/kg, IM). A midline incision was made in the neck to expose and isolate the left carotid and right jugular. The left carotid artery was cannulated with a 24 ga/0.75 in angiocath catheter for the withdrawal of blood samples. The right jugular vein was cannulated with saline-filled PE50 tubing for administration of the compound or vehicle. The left femoral vein was isolated and cannulated with saline-filled PE50 tubing for administration of thromboplastin. For thrombus formation, a ventral midline incision was made, and the descending vena cava was carefully exposed and separated from the aorta. Just distal to the renal veins, a suture was looped under the vena cava, and a second loop was placed around the vena cava just proximal to the iliac veins. The main ilio-lumbar and internal spermatic branches of the vena cava were tied off. At this time, a thrombus was formed by injecting 0.2 mL/kg thromboplastin (ThromboMAX with calcium, Sigma Diagnostics T-9902) into the femoral vein over 10 s followed by a 10 s waiting period. Then, the proximal loop just below the renal veins was tied, and after a 15 min waiting period, the distal loop was tied. At this time, the section of vena cava was removed and carefully cut open followed by removal and weighing of the thrombus.

In the intravenous studies, vehicle (solutol 10% and D5W) or **8** was infused over a 45 min time period at 0.04 mL/min. The total cumulative doses of **8** studied were 0.1, 0.3, and 1.0 mg/kg, iv. The procedure for thrombus formation detailed above was begun at the 30 min point of the infusion. In the oral dose studies, **8** at 10, 30, and 50 mg/kg was solubilized in 0.5% methocel in a total volume of 5 mL/kg and administered by an oral dosing tube. The rats were anesthetized 45 min after the oral dose, and the above thrombus formation procedure was begun

at 70 min postdosing. In both the intravenous and the oral studies, a blood sample was taken at the termination of the experiment to measure coagulation times and drug plasma concentration.

Rat ECAT Model. Male Sprague–Dawley rats (350–450 g) were anesthetized with pentobarbital 65 mg/mL (1 mL/kg, i.p.). A midline incision was made in the neck to expose and isolate the blood vessels. The right carotid artery was cannulated with a saline-filled PE-50 catheter attached to a statham pressure transducer to measure blood pressure and heart rate. The left carotid artery was isolated, and a pulsed Doppler flow probe (HVPD-20, Crystal Biotech, Hopkinton, MA) was placed distally on the artery to measure blood flow. The left jugular vein was cannulated for administration of the compound or vehicle. To prevent thrombosis, the arterial catheters were coated with Sigmacote and air-dried. Proximal to the flow probe, the carotid artery was laid across the exposed electrode wire in the hook end of a bipolar Dastre electrode (Harvard Apparatus, Holliston, MA). The electrode was fitted onto a micromanipulator and positioned with slight upward tension but so that flow was unaffected.

Once a steady baseline blood flow was achieved, solutol vehicle (10%) or **8** (0.03, 0.1, 0.3, or 1.0 mg/kg) was administered by slow infusion into the left jugular vein for 20 min at a rate of 0.05 mL/min. Electrical stimulation was begun after 5 min of infusion and continued for 5 min. The flow crystal sensor was turned off for the duration of electrical stimulation. Occlusion times were recorded during the 30 min observation period beginning at the conclusion of electrical stimulation. Differences in time to occlusion between compound-treated and vehicle-treated rats were compared using an unpaired *t* test. $P < 0.05$ was considered statistically different.

Dog Arteriovenous Shunt Model. Adult mongrel dogs of either sex (13.2–14.5 kg) were dosed with vehicle or **8** or **7**. Following a 1 h observation period, the dogs were anesthetized with pentobarbital sodium (35 mg/kg, iv) and ventilated with room air via an endotracheal tube (15 strokes/min, 25 mL/kg). The heart rate was monitored using a cardiometer triggered from a lead II electrocardiogram generated by limb leads. A Millar pressure-tipped catheter (Millar Instruments, Houston, TX) was placed in the left femoral artery for measurement of blood pressure. A carotid artery was cannulated (PE-200) for blood withdrawal. The right femoral artery and the right femoral vein were cannulated with silicon-treated saline-filled polyethylene tubing (PE-200) and connected with a 6 cm section of silicon-treated tubing (PE-240) to form an extracorporeal arteriovenous shunt. The shunt patency was monitored using a Doppler flow system and flowprobe (2.4–2.8 mm) placed proximal to the locus of the shunt. All parameters were monitored continuously using an LDS PoNeMah Life Science Suite data acquisition system (LDS Test and Measurement, Middleton, WI). On completion of a 15 min postsurgical stabilization period, an occlusive thrombus was formed by the introduction of a thrombogenic surface (0 braided silk thread, 6 cm in length, Ethicon Inc., Somerville, NJ) into the shunt. Seven 15 min shunt periods were employed with the first starting at 2 h postoral dosing and repeated every 30 min out to 5 h postdrug. At the end of each 15 min shunt period, the silk was carefully removed and weighed. The thrombus weight was calculated by subtracting the weight of the silk (9 mg) prior to placement from the total wet weight of the silk on removal from the shunt. Arterial blood was withdrawn prior to the oral dose and at 2–5 h postdrug for determination of aPTT. The template bleeding time was also performed at 2–5 h postdrug by making an incision into the gum (Surgicutt, ITC Corp., Edison, NJ), and the time to clot formation was monitored. Coagulation parameters were determined using plasma in an ACL-100 micro-sampler coagulation analyzer. Plasma samples were measured for drug plasma concentration.

References

- (1) (a) Lilienfeld, D. E.; Chan, E.; Ehland, J.; Godbold, J. H.; Landrigan, P. J.; Marsh, G. Mortality from pulmonary embolism in the United States: 1962 to 1984. *Chest* **1990**, *98*, 1067–1072. (b) Lilienfeld, D. E. Decreasing mortality from pulmonary embolism in the United States, 1979–1996. *Int. J. Epidemiol.* **2000**, *29*, 465–469.
- (2) Melnikova, I. The anticoagulants market. *Nat. Rev. Drug Discovery* **2009**, *8*, 353–354.
- (3) Halperin, J. L. Ximelagatran: Oral direct thrombin inhibition as anticoagulant therapy in atrial fibrillation. *J. Am. Coll. Cardiol.* **2005**, *45*, 1–9.
- (4) (a) Borrissoff, J. I.; Spronk, H. M. H.; Heeneman, S.; ten Cate, H. Is thrombin a key player in the 'coagulation-antherogenesis' maze? *Cardiovasc. Res.* **2009**, *82*, 392–403. (b) Tanaka, K. A.; Key, N. S.; Levy, J. H. Blood coagulation: Hemostasis and thrombin regulation. *Anesth. Analg.* **2009**, *108*, 1433–1446. (c) Santilli, F.; Dav, G. Thrombin as a common downstream target blocking both platelet and monocyte activation. *Thromb. Haemostasis* **2009**, *101*, 220–221.
- (5) Sambrano, G. R.; Weiss, E. J.; Zheng, Y. W.; Huang, W.; Soughlin, S. R. Role of thrombin signaling in platelets in haemostasis and thrombosis. *Nature* **2001**, *413*, 74–78.
- (6) Crowther, M. A.; Weitz, J. I. Ximelagatran: The first oral direct thrombin inhibitor. *Expert Opin. Invest. Drugs* **2004**, *13*, 403–413.
- (7) Patterson, C.; Stouffer, G. A.; Madamanchi, N.; Runge, M. S. New tricks for old dogs: Nonthrombotic effects of thrombin in vessel wall biology. *Circ. Res.* **2001**, *88*, 987–997.
- (8) Fleitz, F. J.; Lyle, T. A.; Zheng, N.; Armstrong, J. D.; Volante, R. P. Kilogram scale synthesis of the pyrazinone acetic acid core of an orally efficacious thrombin inhibitor. *Synth. Commun.* **2000**, *30*, 3171–3180.
- (9) (a) Chung, J. Y. L.; Cvetovick, R. J.; Tsay, F.-R.; Dormer, P. G.; DiMichele, L.; Mathre, D. J.; Chilenski, J. R.; Mao, B.; Wenslow, R. Synthesis of 3-aminopyrazinone mediated by 2-pyridylthioimide-ZnCl₂ complexes. Development of an efficient route to a thrombin inhibitor. *J. Org. Chem.* **2003**, *68*, 8838–8846. (b) Burgey, C. S.; Robinson, K. A.; Williams, P. D.; Coburn, C. A.; Lyle, T. A.; Sanderson, P. E. PCT Int. Appl. WO 0075134, **2000**. (c) CAUTION! Solid bromopyrazinone is known to be thermally unstable with an exothermic transition at 50 °C, is potentially shock sensitive, and gradually decomposes at room temperature.
- (10) (a) Costanzo, M. J.; Maryanoff, B. E.; Hecker, L. R.; Schott, M. R.; Yabut, S. C.; Zhang, H.-C.; Andrade-Gordon, P.; Kaufmann, J. A.; Lewis, J. M.; Krishnan, R.; Tulinsky, A. Potent thrombin inhibitors that probe the S1' subsite: Tripeptide transition state analogues based on a heterocycle-activated carbonyl group. *J. Med. Chem.* **1996**, *39*, 3039–3043. (b) Costanzo, M. J.; Almond, H. R., Jr.; Hecker, L. R.; Schott, M. R.; Yabut, S. C.; Zhang, H.-C.; Andrade-Gordon, P.; Corcoran, T. W.; Giardino, E. C.; Kaufmann, J. A.; Lewis, J. M.; de Garavilla, L.; Haertlein, B. J.; Maryanoff, B. E. In-depth study of tripeptide-based α -keto-heterocycles as inhibitors of thrombin. Effective utilization of the S1' subsite and its implications to structure-based drug design. *J. Med. Chem.* **2005**, *48*, 1984–2008.
- (11) Brown, F. J.; Andisik, D. W.; Bernstein, P. R.; Bryant, C. B.; Ceccarelli, C.; Damewood, J. R., Jr.; Edwards, P. D.; Ealey, R. A.; Feeney, S.; Green, R. C.; Gomes, B.; Kosmider, B. J.; Krell, R. D.; Shaw, A.; Steelman, G. B.; Thomas, R. M.; Vacek, E. P.; Veale, C. A.; Tuthill, P. A.; Warner, P.; Williams, J. C.; Wolanin, D. J.; Woolson, S. A. Design of orally active, non-peptidic inhibitors of human leukocyte elastase. *J. Med. Chem.* **1994**, *37*, 1259–1261.
- (12) Sanderson, P. E. J.; Lyle, T. A.; Cutrona, K. J.; Dyer, D. L.; Dorsey, B. D.; McDonough, C. M.; Naylor-Olsen, A. M.; Chen, I.-W.; Chen, Z.; Cook, J. J.; Cooper, C. M.; Gardell, S. J.; Hare, T. R.; Krueger, J. A.; Lewis, S. D.; Lin, J. H.; Lucas, B. J., Jr.; Lyle, E. A.; Lynch, J. J., Jr.; Stranieri, M. T.; Vastag, K.; Yan, Y.; Shafer, J. A.; Vacca, J. P. Efficacious, orally bioavailable thrombin inhibitors based on 3-aminopyridone or 3-aminopyrazinone acetamide peptidomimetic templates. *J. Med. Chem.* **1998**, *41*, 4466–4474.
- (13) Isaacs, R. C. A.; Solinsky, M. G.; Cutrona, K. J.; Newton, C. L.; Naylor-Olsen, A. M.; Krueger, J. A.; Lewis, S. D.; Lucas, B. J. Structure-based design of novel groups for use in the P1 position of thrombin inhibitor scaffolds. Part I: Weakly basic azoles. *Bioorg. Med. Chem. Lett.* **2000**, *16*, 338–342.
- (14) Tomczuk, B.; Lu, T.; Soll, R. M.; Fedde, C.; Wang, A.; Murphy, L.; Crysler, C.; Dasgupta, M.; Eisennagel, S.; Spurlino, J.; Bone, R. Oxyguanidines: Application to non-peptide phenyl-based thrombin inhibitors. *Bioorg. Med. Chem. Lett.* **2003**, *13*, 1495–1498.
- (15) Burgey, C. S.; Robinson, K. A.; Lyle, T. A.; Nantermet, P. G.; Selnick, H. G.; Isaacs, R. C. A.; Lewis, S. D.; Lucas, B. J.; Krueger, J. A.; Singh, R.; Miller-Stein, C.; White, R. B.; Wong, B.; Lyle, E. A.; Stranieri, M. T.; Cook, J. J.; McMasters, D. R.; Pellicore, J. M.; Pal, S.; Wallace, A. A.; Clayton, F. C.; Bohn, D.; Welsh, D. C.; Lynch, J. J., Jr.; Yan, Y.; Chen, Z.; Kuo, L.; Gardell, S. J.; Shafer, J. A.; Vacca, J. P. Pharmacokinetic optimization of 3-amino-6-chloropyrazinone acetamide thrombin inhibitors. Implementation of P3 pyridine N-oxides to deliver an orally bioavailable series containing P1 N-benzylamines. *Bioorg. Med. Chem. Lett.* **2003**, *13*, 1353–1357.
- (16) (a) Riffel, K. A.; Hengchang, S.; Gu, X.; Yan, K.; Lo, M.-W. Simultaneous determination of a novel thrombin inhibitor and its two metabolites in human plasma by liquid chromatography/tandem mass spectrometry. *J. Pharm. Biomed. Anal.* **2000**, *23*, 607–616. (b) Burgey, C. S.; Robinson, K. A.; Lyle, T. A.; Sanderson, P. E. J.; Lewis, S. D.; Lucas, B. J.; Krueger, J. A.; Singh, R.; Miller-Stein, C.; White, R. B.; Wong, B.; Lyle, E. A.; Williams, P. D.; Coburn, C. A.; Dorsey, B. D.; Barrow, J. C.; Stranieri, M. T.; Holahan, M. A.; Sitko, G. R.; Cook, J. J.; McMasters, D. R.; McDonough, C. M.; Sanders, W. M.; Wallace, A. A.; Clayton, F. C.; Bohn, D.; Leonard, Y. M.; Detwiler, T. J.; Lynch, J. J.; Yan, Y.; Chen, Z.; Kuo, L.; Gardell, S. J.; Shafer, J. A.; Vacca, J. P. Metabolism-directed optimization of 3-aminopyrazinone acetamide thrombin inhibitors. Development of an orally bioavailable series containing P1 and P3 pyridines. *J. Med. Chem.* **2003**, *46*, 461–473.
- (17) Young, M. B.; Barrow, J. C.; Glass, K. L.; Lundell, G. F.; Newton, C. L.; Pellicore, J. M.; Rittle, K. E.; Selnick, H. G.; Stauffer, K. J.; Vacca, J. P.; Williams, P. D.; Bohn, D.; Clayton, F. C.; Cook, J. J.; Krueger, J. A.; Kuo, L. C.; Lewis, S. D.; Lucas, B. J.; McMasters, D. R.; Miller-Stein, C.; Pietrak, B. L.; Wallace, A. A.; White, R. B.; Wong, B.; Yan, Y.; Nantermet, P. G. Discovery and evaluation of potent P1 aryl heterocycle-based thrombin inhibitors. *J. Med. Chem.* **2004**, *47*, 2995–3008.
- (18) Lu, T.; Markotan, T.; Coppo, F.; Tomczuk, B.; Crysler, C.; Eisennagel, S.; Spurlino, J.; Gremminger, L.; Soll, R. M.; Giardino, E. C.; Bone, R. Oxyguanidines. Part 2: Discovery of a novel orally active thrombin inhibitor through structure-based drug design and parallel synthesis. *Bioorg. Med. Chem. Lett.* **2004**, *14*, 3727–3731.
- (19) (a) Walkowiak, J.; Witmanowski, H.; Strzykała, K.; Bychowicz, B.; Songin, T.; Borski, K.; Herzig, K.-H. Inhibition of endogenous pancreatic enzyme secretion by oral pancreatic enzyme treatment. *Eur. J. Clin. Invest.* **2003**, *33*, 65–69. (b) Obour, J. D.; Frame, S. R.; Shiu, T.; Solomon, T. E.; Cook, J. C. Evidence that A8947 enhances pancreas growth via a trypsin inhibitor mechanism. *Toxicol. Appl. Pharmacol.* **1997**, *146*, 116–126.
- (20) Chen, Z.; Li, Y.; Mulichak, A. M.; Lewis, S. D.; Shafer, J. A. Crystal structure of human α -thrombin complexed with hirugen and p-amidinophenylpyruvate at 1.6 Å resolution. *Arch. Biochem. Biophys.* **1995**, *322*, 198–203.
- (21) Sanderson, P. E.; Stanton, M. G.; Dorsey, B. D.; Lyle, T. A.; McDonough, C.; Sanders, W. M.; Savage, K. L.; Naylor-Olsen, A. M.; Krueger, J. A.; Lewis, S. D.; Lucas, B. J.; Lynch, J. J.; Yan, Y. Azaindoles: Moderately basic P1 groups for enhancing the selectivity of thrombin inhibitors. *Bioorg. Med. Chem. Lett.* **2003**, *13*, 795–798.
- (22) Isaacs, R. C. A.; Solinsky, M. G.; Cutrona, K. J.; Newton, C. L.; Naylor-Olsen, A. M.; Krueger, J. A.; Lewis, S. D.; Lucas, B. J. Structure-based design of novel groups for use in the P1 position of thrombin inhibitor scaffolds. Part I: Weakly basic azoles. *Bioorg. Med. Chem. Lett.* **2006**, *16*, 338–342.
- (23) Isaacs, R. C. A.; Solinsky, M. G.; Cutrona, K. J.; Newton, C. L.; Naylor-Olsen, A. M.; McMasters, D. R.; Krueger, J. A.; Lewis, S. D.; Lucas, B. J.; Kuo, L. C.; Yan, Y.; Lynch, J. J.; Lyle, E. A. Structure-based design of novel groups for use in the P1 position of thrombin inhibitor scaffolds. Part 2: N-acetamidoimidazoles. *Bioorg. Med. Chem. Lett.* **2008**, *18*, 2062–2066.
- (24) Reiner, J. E.; Siev, D. V.; Araldi, G.-L.; Cui, J. J.; Ho, J. Z.; Reddy, K. M.; Mamedova, L.; Vu, P. H.; Lee, K.-S. S.; Minami, N. K.; Gibson, T. S.; Anderson, S. M.; Bradbury, A. E.; Nolan, T. G.; Semple, J. E. Non-covalent thrombin inhibitors featuring P3-heterocycles with P1-monocyclic arginine surrogates. *Bioorg. Med. Chem. Lett.* **2002**, *12*, 1203–1208.
- (25) (a) Schumacher, W. A.; Heran, C. H.; Steinbacher, T. E.; McGill, J. R.; Bird, J. E.; Giancarli, M. R.; Durham, S. K. Thrombin inhibition compared with other antithrombotic drugs in rats. *Thromb. Res.* **1992**, *68*, 157–66. (b) Berry, C. N.; Girard, D.; Lochot, S.; Lecoffre, C. Antithrombotic actions of argatroban in rat models of venous, 'mixed' and arterial thrombosis, and its effects on the tail transection bleeding time. *Br. J. Pharmacol.* **1994**, *113*, 1209–1214. (c) Wong, P. C.; Crain, E. J.; Knabb, R. M.; Meade, R. P.; Quan, M. L.; Watson, C. A.; Wexler, R. R.; Wright, M. R.; Slee, A. M. Nonpeptide factor Xa inhibitors II. Antithrombotic evaluation in a rabbit model of electrically induced carotid artery thrombosis. *J. Pharmacol. Exp. Ther.* **2000**, *295*, 212–218.
- (26) Giardino, E. C.; Costanzo, M. J.; Kauffman, J. A.; Li, Q.-S.; Maryanoff, B. E.; Andrade-Gordon, P. Antithrombotic properties

- of RWJ-50353, a potent and novel thrombin inhibitor. *Thromb. Res.* **2000**, *98*, 83–93.
- (27) Barrett, J. A.; Crocker, A. C.; Damphousse, D. J.; Heminway, S. J.; Liu, S.; Edwards, D. S.; Lazewatsky, J. L.; Kagan, M.; Mazaika, T. J.; Carroll, T. R. Biological evaluation of thrombus imaging agents utilizing water soluble phosphines and tricine as coligands when used to label a hydrazinonicotinamide-modified cyclic glycoprotein IIb/IIIa receptor antagonist with ^{99m}Tc . *Bioconjugate Chem.* **1997**, *8*, 155–160.
- (28) Lorrain, J.; Millet, L.; Lechaire, I.; Lochot, S.; Ferrari, P.; Visconte, C.; Sainte-Marie, M.; Lunven, C.; Berry, C. N.; Schaeffer, P.; Herbert, J.-M.; O'Connor, S. E. Antithrombotic properties of SSR182289A, a new, orally active thrombin inhibitor. *J. Pharmacol. Exp. Ther.* **2003**, *304*, 567–574.
- (29) Lu, T.; Tomczuk, B. T.; Markotan, T. P. U.S. Patent 6,204, 263 B1, 2001.
- (30) Cheng, Y.; Prusoff, W. H. Relationship between the inhibition constant (K_i) and the concentration of inhibitor which causes 50% inhibition (IC_{50}) of an enzymatic reaction. *Biochem. Pharmacol.* **1973**, *22*, 3099–3108.
- (31) (a) Webber, P. C.; Lee, S.-L.; Lewandowski, F. A.; Schadt, M. C.; Chang, C.-H.; Kettner, C. A. Kinetic and crystallographic studies of thrombin with Ac-(D)Phe-Pro-boroArg-OH and its lysine, amidine, homolysine and ornithine analogs. *Biochemistry* **1995**, *34*, 3750–3757. (b) Skrzypczak-Jankun, E.; Carperos, V.; Ravichandran, K. G.; Tulinsky, A.; Westbrook, M.; Maraganore, J. M. Structure of the hirugen and hirulog 1 complexes of α -thrombin. *J. Mol. Biol.* **1991**, *221*, 1379–1393.
- (32) Brunger, A. T.; Kuriyan, J.; Karplus, M. Crystallographic R-factor refinement by molecular dynamics. *Science* **1987**, *235*, 458–460.
- (33) Bernstein, F. C.; Koetzle, T. F.; Meyer, E. F., Jr.; Brice, M. D.; Rodgers, J. R.; Kennard, O.; Shimanouchi, T.; Tasumi, M. The protein databank: A computer based archival file for macromolecular structures. *J. Mol. Biol.* **1977**, *112*, 535–542.
- (34) Sack, J. S. CHAIN—A crystallographic modeling program. *J. Mol. Graphics* **1988**, *249*, 224–225.